POLITECNICO DI TORINO
Repository ISTITUZIONALE

EnergyBased Semiactive Control Algorithms for Nonlinear Framed Structures Using the Force Analogy Method

Original
EnergyBased Semiactive Control Algorithms for Nonlinear Framed Structures Using the Force Analogy Method / De Iuliis, M., Miceli, E., Castaldo, P.. - In: STRUCTURAL CONTROL & HEALTH MONITORING. - ISSN 1545-2255. - 2026:(2026), pp. 1-29. [10.1155/stc/8260623]

Availability:
This version is available at: 11583/3018018 since: 2026-11-17T13:47:34Z

Publisher:
John Wiley and Sons

Published
DOI:10.1155/stc/8260623

Terms of use:

This article is made available under terms and conditions as specified in the corresponding bibliographic description in the repository

Publisher copyright

(Article begins on next page)

29 November 2026

Check for updates

Structural Control and Health Monitoring

WILEY

RESEARCH ARTICLE OPEN ACCESS

Energy-Based Semiactive Control Algorithms for Nonlinear Framed Structures Using the Force Analogy Method

M. De Iuliis | E. Miceli | P. Castaldo

Department of Structural, Geotechnical and Building Engineering (DISEG), Politecnico Di Torino, Turin, Italy

Correspondence: M. De Iuliis (massimiliano.deiuliis@polito.it)

Received: 6 January 2026 | **Revised:** 3 May 2026 | **Accepted:** 8 June 2026

Academic Editor: Łukasz Jankowski

Keywords: damage mitigation | energy-based structural control | force analogy method | nonlinear moment-resisting framed structure | semiactive control

ABSTRACT

This study presents a novel framework for developing closed-form semiactive control algorithms specifically designed for structures exhibiting inelastic response during seismic events. The proposed approach leverages the force analogy method (FAM) to represent structural nonlinearity through equivalent forces rather than continuous stiffness matrix updates, enabling efficient real-time computation. Five distinct energy-based control strategies are formulated: maximization of dissipated energy, minimization of elastic energy, minimization of hysteretic energy, minimization of kinetic energy, and minimization of input energy. Each algorithm provides explicit control laws for adjusting both damping and stiffness properties of semiactive devices based on instantaneous structural response quantities. These algorithms have been tested through an extensive numerical investigation on two benchmark steel moment-resisting frames (3-story and 9-story buildings) subjected to 85 natural seismic records with diverse dynamic characteristics, including both far-field and near-fault ground motions. The effectiveness of the proposed strategies was evaluated by comparing the seismic responses in terms of both relative displacement and energy components, with the regular configuration of semiactive devices (i.e., passive control) and other algorithms, such as "Kamagata and Kobori" and "Sky–Hook," finalized, respectively, to manage stiffness and damping extrastructural resources. The energy-based optimization approach constitutes the unifying theoretical basis of the proposed framework, enabling the systematic derivation of physically interpretable control laws tailored to specific seismic performance targets. The computational efficiency of the resulting algorithms makes them well suited for practical implementation in real-world structural control applications.

1 | Introduction

The protection of civil structures against seismic events remains one of the most significant challenges in structural engineering, especially considering the age of most of the building stock, even in areas characterized by high seismic hazard. In such locations, seismic events can generate seismic demand that exceeds the elastic response capacity of the structural system's components, leading to permanent deformations, local damage, and, in the worst cases, global collapse. For a large share of the existing building stock, designed to less demanding standards, inelastic structural response under moderate-to-strong ground motions is not a marginal possibility but a foreseeable behavior. This makes the problem of controlling structures in the nonlinear range an issue of primary practical relevance, one that the structural control community has so far addressed only partially. In this context, the use of active and semiactive external devices to control the structural response during seismic excitation has become a well-established and continuously evolving research field. The present work contributes to this field by proposing a novel framework for the semiactive control of framed structures operating in the nonlinear range, leveraging the force

This is an open access article under the terms of the Creative Commons Attribution License, which permits use, distribution and reproduction in any medium, provided the original work is properly cited.

Copyright © 2026 M. De Iuliis et al. *Structural Control and Health Monitoring* published by John Wiley & Sons Ltd.

analogy method (FAM) as theoretical substrate for deriving new, closed-form, energy-based control algorithms.

Structural control strategies for seismic applications are traditionally classified into three main categories: passive, active, and semiactive controls [1]. Passive systems, such as viscous dampers, base isolators, and friction or metallic dampers, require no external energy and have been widely adopted for their simplicity and reliability [2–4]. Active control systems achieve higher performance by applying computed forces in real time but at the cost of significant energy demand, hardware complexity, and potential instability arising from signal delays, model uncertainties, and actuator saturation [5–7]. A fundamental assumption underlying most active control formulations, however, is that the controlled structure behaves elastically or can be adequately linearized, an assumption that may not hold when strong ground motions lead the structure to the inelastic range.

Semiactive control represents a physically consistent compromise, being able to modify their mechanical properties in real time with minimal energy input [8, 9], combining the reliability of passive systems with part of the adaptability of active ones [10–14].

Among the semiactive technologies, magnetorheological (MR) dampers [15, 16] have been widely applied to multistory structures for damping control, owing to their fast response time and broad force range. Semiactive friction dampers represent an alternative solution for energy dissipation control, in which the slip force is adjusted in real time through a controllable normal force [17], with the nonlinear frictional behavior being reducible to an equivalent viscous representation through established linearization procedures. Variable stiffness devices, including variable orifice fluid dampers and actively controlled bracing systems, allow the lateral stiffness of the structural system to be modified in real time [18–20], while negative stiffness devices [21] extend the controllable stiffness range beyond zero, offering additional flexibility in tailoring the structural dynamic response. Despite the diversity of available technologies, a common feature of all these devices is that their controllable mechanical properties, i.e., equivalent damping coefficient and equivalent stiffness, can be adjusted between prescribed bounds through appropriate characterization procedures [22–24].

A crucial role in the effectiveness of semiactive control systems is linked to the control algorithm used. The most common proposals in the literature refer to clipped-optimal algorithms, which approximate the optimal active control law while taking into account the technological constraints of the actuators [15, 16]; bang–bang algorithms, which simply activate or deactivate the device based on a discrete set of operating modes [25]; algorithms based on Lyapunov stability theory, where an energy functional is constructed that the control law must make decreasing [26, 27]; or algorithms that utilize the skyhook principle, where damping is applied proportionally to the relative velocity with respect to a fixed virtual reference point in space, rather than to the structure itself [27, 28]. Over time, more complex approaches have been proposed that involve the use of artificial intelligence tools, fuzzy logic, and neural networks. Specifically, Zhi and Olotunde [29] implemented an Adaptive Neurofuzzy Inference System (ANFIS) controller, optimizing the fuzzy parameters based on the structural response and achieving a reduction in the seismic response compared to the uncontrolled cases. Recently, Xiao et al. [30] proposed an "intelligent" semiactive algorithm with seismic reliability learning and evaluation via probability density evolution, demonstrating that the algorithm improves the system's robustness compared to conventional control. Despite this diversity of approaches, a common limitation shared by virtually all these algorithms is their implicit or explicit reliance on linear or linearized structural models. When inelastic deformations occur, the energy balance of the system changes fundamentally: stiffness degrades, hysteretic dissipation redistributes across yielded members, and control laws calibrated on elastic assumptions may systematically misallocate control resources, precisely in the scenarios where effective mitigation is most needed.

Alongside these algorithmic shortcomings, the practical use of semiactive devices remains subject to several implementation uncertainties: delays in actuators and control systems, measurement errors, model approximations, saturation phenomena, and computational complexity. The lack of nonlinearity-consistent control algorithms becomes particularly critical for the existing building stock, where inelastic excursions are expected under design-level ground motions. Addressing it requires algorithms that are explicitly formulated for nonlinear structural behavior, computationally efficient enough for real-time implementation, and physically interpretable so that their control actions can be related to meaningful energy quantities and verified by engineers.

Analyzing and managing the nonlinear behavior of a structure under seismic loading is a classic research topic that remains relevant due to its importance in performance-based seismic design and damage control methods. Traditional numerical techniques such as nonlinear incremental analysis, implicit or explicit integration, Newton–Raphson methods, and tangent matrix updates are efficient but can become computationally expensive for real-time simulations or large-scale evaluations of many scenarios [31]. The FAM, originally conceived by Lin [32], proposes a different approach: representing structural nonlinearity not by continuously updating the stiffness matrix but by assuming it remains constant, while the nonlinearity component is incorporated into the internal force vector, adding equivalent plastic forces that cause the structure to deform as it would actually in the nonlinear field [33]. This approach shifts the burden of handling nonlinearity from continuously updating matrices to calculating equivalent perturbations on forces and displacements, a property that proves particularly valuable in the context of real-time control loops, where stiffness matrix updates at each time step would introduce computationally unacceptable overhead and algorithmic complexity. Several studies have verified the reliability and accuracy of the FAM. Calofir et al. [34] used this approach to study the behavior of a 10-story-reinforced concrete structure subjected to recorded seismic excitations, positively comparing the results with commercial software. Patlán et al. [35] instead focused on the computational efficiency of the algorithm, proposing a new temporal integration scheme, while Toloue et al. [36] showed that the use of Timoshenko elements within the FAM, in the case of large plastic rotations, can better reproduce experiments compared to traditional Euler–Bernoulli theory, with accuracies up to 98%. An interesting extension is the application of the FAM to the case where the structural system exhibits geometric nonlinearities [37]. In this formulation, the estimation of the dynamic response

scihm, 2026, 1, Downloaded from https://onlinelibrary.wiley.com/doi/10.1155/stc/8260623 by M. De Iuliis - Politecnico Di Torino Sist. Bibl Del Polit Di Torino , Wiley Online Library on [13/08/2026]. See the Terms and Conditions (https://onlinelibrary.wiley.com/terms-and-conditions) on Wiley Online Library for rules of use; OA articles are governed by the applicable Creative Commons License

is obtained both through the equivalent forces used to address material nonlinearities and through the updating of stiffnesses for geometric effects. Taken together, these studies establish FAM as an accurate, generalizable, and computationally efficient method for nonlinear dynamic analysis. Within the framework of structural control, its fixed-stiffness formulation serves as a methodological bridge: it allows the nonlinear behavior of the structure under control to be represented as an "equivalent structure" with constant stiffness modified by analogous forces, making controller design simpler, avoiding the continuous updating of the system's stiffness properties, and improving computational robustness in real-time environments. Nevertheless, the explicit use of FAM as the theoretical foundation for deriving closed-form semiactive control laws, rather than simply as a simulation tool, remains largely unexplored [38, 39]. In particular, no prior work has combined the FAM framework with an energy-based control formulation to derive algorithms that are simultaneously nonlinearity consistent, computationally efficient, and physically interpretable.

The present paper addresses this gap by deriving five novel closed-form semiactive control algorithms explicitly formulated for nonlinear framed structures within the FAM framework, each targeting a distinct component of the structural energy balance: the maximization of dissipated energy as well as the minimization of elastic, hysteretic, kinetic, and input energy rates. The energy-based nature of the proposed formulation connects this work to a broader line of research on energy-driven control strategies. Existing approaches in this family, however, are predominantly formulated for linear or base-isolated structural systems, including energy based semiactive control for linear asymmetric one-way structures [39, 40], absolute-energy-based active control laws for linear isolation systems [41], energy-based predictive algorithms for semiactive tuned mass dampers on linear structures [42], and instantaneous minimum input energy strategies for isolation systems with covarying stiffness and damping [43]. A related contribution [44] combined the FAM with an energy analysis of inelastic structures equipped with passive tuned mass dampers, demonstrating the natural compatibility between FAM and energy-based response characterization, yet without extending this framework to the derivation of semiactive control laws. The linearity assumption underlying most of these approaches is not incidental: as explicitly acknowledged in [45], energy-based semiactive controllers applied to multistory structures with MR dampers assume that the structural response remains in the elastic range and that a different formulation is required for the nonlinear case. The present work advances this line of research by generalizing the energy-based control formulation to multistory moment-resisting frames (MRFs) with distributed nonlinearity, integrating it with the FAM to achieve closed-form, nonlinearity-consistent control laws suitable for real-time implementation without iterative procedures. The physical interpretability of the energy-based formulation further distinguishes the proposed approach from control strategies relying on more opaque mathematical constructs, as each control action retains a direct and verifiable meaning in terms of the structural energy balance.

The algorithms identified in this way will be tested on scientifically recognized benchmark models for the nonlinear system control problem [46]. To ensure the robustness and generality of the method, a wide range of seismic excitations with different dynamic characteristics (i.e., far-field [FF] and near-fault [NF]) will be considered, evaluating the performance of the proposed control laws with reference to response parameters related to the damage level of the structural system, both compared to the uncontrolled system and to algorithms with the same level of computational complexity.

Based on the above, the paper is organized as follows. Section 2 presents the essential theoretical elements of the FAM and characterizes the dynamic problem in terms of energy rates. Section 3 illustrates the mathematical derivation of the proposed semiactive control algorithms. Section 4 briefly describes the properties of the benchmark structures and seismic excitations considered in the numerical investigation, whose results are presented in Section 5. Finally, Section 6 concludes with a critical assessment of the effectiveness and robustness of the proposed control algorithms.

2 | Basic Elements of the FAM

The FAM, originally proposed by Lin [32] and further developed in [33], represents structural nonlinearity through equivalent plastic forces acting on a system of constant stiffness rather than by updating the stiffness matrix at each time step. For a MRF with n degrees of freedom and m potential plastic hinge locations, the method yields the following characteristic equation relating the total moment vector at the plastic hinge locations to the total displacement vector and the plastic rotation vector:

$$M^{tot}(t) = K_P^T \cdot X(t) - K_R \cdot \theta^{\text{inel}}(t). \tag{1}$$

Together with the constitutive relationship of the plastic hinges, $M^{\text{tot}}(t) = f(\theta^{\text{inel}}(t))$, Equation (1) allows the total moment vector and the corresponding plastic rotations to be evaluated from the total displacement vector at each time step, without updating the structural stiffness matrix. The reader is referred to [32, 33] for the complete derivation.

In this framework, the total displacement vector is decomposed as follows:

$$\mathrm{X}(t) = \mathrm{X}^{el}(t) + \mathrm{X}^{\text{inel}}(t), \tag{2}$$

where $\mathrm{X}^{el}(t)$ denotes the elastic component, recovered upon unloading, and $\mathrm{X}^{\text{inel}}(t)$ is the inelastic component, arising from plastic rotations that develop at specific locations within the structure once the elastic limit is exceeded. The effect of these plastic rotations is represented through equivalent forces acting on the system of constant stiffness so that the inelastic displacement can be expressed as follows:

$$\mathrm{X}^{\text{inel}}(t) = \mathrm{K}^{-1}\mathrm{K}_P\theta^{inel}(t), \tag{3}$$

and the elastic displacement is obtained by subtraction using Equation (2).

The nonlinear behavior of systems subjected to dynamic loads can be studied, within the FAM framework, by simply considering that while the inertial and damping forces are related to the total displacement, the elastic action refers only to the elastic

schm, 2026, 1, Downloaded from https://onlinelibrary.wiley.com/doi/10.1155/stc/8260623 by M. De Iuliis - Politecnico Di Torino Sist. Bibl Del Polit Di Torino , Wiley Online Library on [13/08/2026]. See the Terms and Conditions (https://onlinelibrary.wiley.com/terms-and-conditions) on Wiley Online Library for rules of use; OA articles are governed by the applicable Creative Commons License

component of that displacement. For a system with n degrees of freedom, the matrix equation representing the seismic dynamics of the system can thus be written as follows:

$$\mathrm{M}\cdot\ddot{\mathrm{X}}(t)+\mathrm{C}\cdot\dot{\mathrm{X}}(t)+\mathrm{K}\cdot\mathrm{X}^{\mathrm{el}}(t)=-\mathrm{M}\cdot\ddot{\mathrm{U}}_g(t), \tag{4}$$

where M is the mass matrix, C the damping matrix, $\ddot{\mathrm{X}}(t)$, $\dot{\mathrm{X}}(t)$, and $\ddot{\mathrm{U}}_g(t)$ represent, respectively, the relative acceleration, the relative velocity, and the ground acceleration at the base, associated with the different degrees of freedom.

It is worth noting that the stiffness term involves $\mathrm{X}^{el}(t)$, the elastic component only, since the restoring force is computed on a system of constant stiffness and reflects only the recoverable part of the deformation. The inertial and damping terms, on the other hand, involve the total displacement $\mathrm{X}(t)$, which encompasses both the elastic and inelastic contributions. This is the distinctive feature of the FAM equation of motion with respect to the conventional linear dynamic equation: the structure is formally treated as elastic, but the full nonlinear response is recovered through the decomposition in Equation (2), where the inelastic part is continuously updated based on the plastic rotations at the potential hinge locations. The integration of Equation (4) allows for the evaluation of the system's dynamic response and the computation of the corresponding energy components at each instant of time.

In order to derive control-oriented expressions, the equation of motion is reformulated in terms of instantaneous power contributions associated with the different energy components. Having this aim, the various energy terms associated with each individual contribution are multiply by $d\mathrm{X}(t)$, obtaining

$$\ddot{\mathrm{X}}^{T}(t)\cdot\mathrm{M}\cdot d\mathrm{X}(t)+\dot{\mathrm{X}}^{T}(t)\cdot\mathrm{C}\cdot d\mathrm{X}(t)+\mathrm{X}^{\mathrm{el}\,T}(t)\cdot\mathrm{K}\cdot d\mathrm{X}(t)=-\ddot{\mathrm{U}}_g^{\,T}(t)\cdot\mathrm{M}\cdot d\mathrm{X}(t). \tag{5}$$

The above formulation is expressed in terms of relative displacements, consistently with the adopted equation of motion, which is written in the ground-fixed reference frame. In the literature, two alternative energy formulations are commonly used, based on either absolute or relative kinematic quantities. As discussed by Uang and Bertero [47], both approaches are physically meaningful, but they differ in the definition of the input energy term. The numerous studies available in the literature, as synthesized in recent state-of-the-art reviews [48], confirm that no formulation can be considered unconditionally preferable and that the choice depends on the specific problem setting. In the present work, the relative formulation is adopted to ensure consistency with the governing equations and the associated energy balance [49].

In the case of the term associated with the elastic force, in order to obtain the infinitesimal variation of the elastic energy, the total displacement is decomposed into its elastic and inelastic components in differential form, namely, $d\mathrm{X}(t)=d\mathrm{X}^{\mathrm{el}}(t)+d\mathrm{X}^{\mathrm{inel}}(t)$, thus allowing Equation (5) to be rewritten as follows:

$$\ddot{\mathrm{X}}^{T}(t)\cdot\mathrm{M}\cdot d\mathrm{X}(t)+\dot{\mathrm{X}}^{T}(t)\cdot\mathrm{C}\cdot d\mathrm{X}(t)+\mathrm{X}^{\mathrm{el}\,T}(t)\cdot\mathrm{K}\cdot d\mathrm{X}^{\mathrm{el}}(t)+\mathrm{X}^{\mathrm{el}\,T}(t)\cdot\mathrm{K}\cdot d\mathrm{X}^{\mathrm{inel}}(t)=-\ddot{\mathrm{U}}_g^{\,T}(t)\cdot\mathrm{M}\cdot d\mathrm{X}(t). \tag{6}$$

By multiplying and dividing each term by dt, the following relation is obtained:

$$\ddot{\mathrm{X}}^{T}(t)\cdot\mathrm{M}\cdot\dot{\mathrm{X}}(t)\cdot dt+\dot{\mathrm{X}}^{T}(t)\cdot\mathrm{C}\cdot\dot{\mathrm{X}}(t)\cdot dt+\mathrm{X}^{\mathrm{el}\,T}(t)\cdot\mathrm{K}\cdot(t)\cdot\dot{\mathrm{X}}^{\mathrm{el}}\cdot dt+\mathrm{X}^{\mathrm{el}\,T}(t)\cdot\mathrm{K}\cdot\dot{\mathrm{X}}^{\mathrm{inel}}(t)\cdot dt=-\ddot{\mathrm{U}}_g^{\,T}(t)\cdot\mathrm{M}\cdot\dot{\mathrm{X}}(t)\cdot dt, \tag{7}$$

where the individual terms that multiply dt represent the instantaneous power associated with the different energy components, specifically $P_K=\ddot{\mathrm{X}}^{T}(t)\cdot\mathrm{M}\cdot\dot{\mathrm{X}}(t)$ kinetic power, $P_\xi=\dot{\mathrm{X}}^{T}(t)\cdot\mathrm{C}\cdot\dot{\mathrm{X}}(t)$ dissipated power, $P_{el}=\mathrm{X}^{\mathrm{el}\,T}(t)\cdot\mathrm{K}\cdot(t)\cdot\dot{\mathrm{X}}^{\mathrm{el}}$ elastic power, $P_{hys}=\mathrm{X}^{\mathrm{el}\,T}(t)\cdot\mathrm{K}\cdot\dot{\mathrm{X}}^{\mathrm{inel}}(t)$ hysteretic dissipated power, and $P_{in}=-\ddot{\mathrm{U}}_g^{\,T}(t)\cdot\mathrm{M}\cdot\dot{\mathrm{X}}(t)$ input power. By introducing these terms, Equation (7) takes the following form:

$$P_K+P_\xi+P_{el}+P_{hys}=P_{in}. \tag{8}$$

3 | Definition of Semiactive Control Algorithms

The possibility of modifying the damping and stiffness matrices in real time through suitable semiactive devices acting directly at the individual degrees of freedom is now considered by introducing the total matrices $\mathrm{C}_{tot}=\mathrm{C}+\Delta\mathrm{C}$ and $\mathrm{K}_{tot}=\mathrm{K}+\Delta\mathrm{K}$, which are substituted into Equation (6). All the proposed control laws are derived following a common procedure: each instantaneous power rate, Equation (8), is expressed in terms of the controllable mechanical properties of the devices and its sensitivity with respect to these parameters is evaluated in order to define a real-time control strategy. For the sake of clarity, the complete derivation is presented only for the dissipated power term, while the same procedure is applied to the remaining energy components in a more compact form.

3.1 | Maximization of Dissipated Power

Consider the term $P_\xi(\mathrm{C}_{tot})$, which can be expressed as follows:

$$P_\xi(\mathrm{C}_{tot})=\dot{\mathrm{X}}^{T}(t)\cdot\mathrm{C}_{tot}\cdot\dot{\mathrm{X}}(t)=\sum_{i=1}^{n}\dot{\mathrm{X}}_i(t)\cdot\left(\sum_{j=1}^{n}\mathrm{C}_{tot,ij}\cdot\dot{\mathrm{X}}_j(t)\right)=\sum_{i=1}^{n}\sum_{j=1}^{n}\mathrm{C}_{tot,ij}\cdot\dot{\mathrm{X}}_i(t)\cdot\dot{\mathrm{X}}_j(t). \tag{9}$$

From a practical standpoint, Equation (9) refers to individual terms of the damping matrix, which do not directly correspond to physical devices. Considering only the contribution associated with the viscous supplemental damping devices, $\Delta\mathrm{C}$, this term does not, in general, correspond to the contribution of a single device, as each device, depending on its operating mechanism, contributes to multiple terms of the matrices in question.

One possible approach to the problem is to define two matrices, which we will refer to as the "force generation matrix," F_C, and the "force localization matrix," B_C, in addition to a diagonal matrix C_d in which the values of the additional viscous damping introduced by each individual device are indicated. The matrix $\Delta\mathrm{C}$ can thus be rewritten in the following form:

$$\Delta\mathrm{C}=\mathrm{B}_C^{\,T}\cdot\mathrm{C}_d\cdot\mathrm{F}_C. \tag{10}$$

The term $\mathrm{C}_d\cdot\mathrm{F}_C\cdot\dot{\mathrm{X}}(t)$ will be a row vector with s elements, containing the forces developed by each individual device, while

scihm, 2026, 1, Downloaded from https://onlinelibrary.wiley.com/doi/10.1155/stc/8260623 by M. De Iuliis - Politecnico Di Torino Sist. Bibl Del Polit Di Torino , Wiley Online Library on [13/08/2026]. See the Terms and Conditions (https://onlinelibrary.wiley.com/terms-and-conditions) on Wiley Online Library for rules of use; OA articles are governed by the applicable Creative Commons License

the matrix B_C will indicate the degrees of freedom to which these forces are applied, along with their respective signs. The matrices F_C and B_C are introduced once and will be used consistently in the following derivations for all energy components.

By rewriting Equation (10) through the introduction of this term, and considering that, since the matrix C_d is diagonal, it follows that

$$\Delta C_{ij} = \sum_{k=1}^{s}\sum_{l=1}^{s} B_{C,ki}\cdot C_{d,kl}\cdot F_{C,lj} = \sum_{l=1}^{s} B_{C,li}\cdot c_l\cdot F_{C,lj}, \tag{11}$$

and this yields

$$\begin{aligned} P_\xi(C_{tot}) &= \sum_{i=1}^{n}\sum_{j=1}^{n}\left(C_{ij} + \sum_{l=1}^{s} B_{C,li}\cdot c_l\cdot F_{C,lj}\right)\cdot \dot{X}_i(t)\cdot \dot{X}_j(t) \\ &= \sum_{i=1}^{n}\sum_{j=1}^{n} C_{ij}\cdot \dot{X}_i(t)\cdot \dot{X}_j(t) + \sum_{\boldsymbol{l=1}}^{\boldsymbol{s}} c_l \\ &\quad \cdot\left(\sum_{i=1}^{n}\sum_{j=1}^{n} B_{C,li}\cdot F_{C,lj}\cdot \dot{X}_i(t)\cdot \dot{X}_j(t)\right). \end{aligned} \tag{12}$$

This expression clearly shows that

$$\Delta P_{\xi,l} = \frac{\partial P_\xi}{\partial c_l}\cdot \Delta c_l = \left(\sum_{i=1}^{n}\sum_{j=1}^{n} B_{C,li}\cdot F_{C,lj}\cdot \dot{X}_i(t)\cdot \dot{X}_j(t)\right)\cdot \Delta c_l. \tag{13}$$

The vector ΔP_ξ, whose l-th component is obtained from Equation (13), contains the sensitivity terms of the dissipated power with respect to the damping that can potentially be applied through the semiactive devices. Since the objective is to maximize the dissipated viscous energy, the strategy consists of maximizing the value of P_ξ, at each instant, which can be achieved through the following control algorithm:

$$\begin{cases} \Delta c_l = \max(\Delta c_l) & \text{if } \sum_{i=1}^{n}\sum_{j=1}^{n} B_{C,li}\cdot F_{C,lj}\cdot \dot{X}_i(t)\cdot \dot{X}_j(t) > 0, \\ \Delta c_l = \min(\Delta c_l) & \text{if } \sum_{i=1}^{n}\sum_{j=1}^{n} B_{C,li}\cdot F_{C,lj}\cdot \dot{X}_i(t)\cdot \dot{X}_j(t) < 0. \end{cases} \tag{14}$$

3.2 | Minimization of the Elastic Power

Following the same procedure described for the dissipated power, the elastic power term, $P_{el}(K_{tot}) = X^{el\,T}(t)\cdot K_{tot}\cdot \dot{X}^{el}(t)$, can be expressed in terms of the controllable stiffness contributions as follows:

$$\begin{aligned} P_{el}(K_{tot}) &= \sum_{\boldsymbol{i=1}}^{\boldsymbol{n}}\sum_{\boldsymbol{j=1}}^{\boldsymbol{n}} K_{ij}\cdot X_i^{el}(t)\cdot \dot{X}_j^{el}(t) + \sum_{\boldsymbol{l=1}}^{\boldsymbol{r}} k_l \\ &\quad \cdot\left(\sum_{i=1}^{n}\sum_{j=1}^{n} B_{K,li}\cdot F_{K,lj}\cdot X_i^{el}(t)\cdot \dot{X}_j^{el}(t)\right), \end{aligned} \tag{15}$$

which leads to the following sensitivity expression:

$$\Delta P_{el,l} = \frac{\partial P_{el}}{\partial k_l}\cdot \Delta k_l = \left(\sum_{i=1}^{n}\sum_{j=1}^{n} B_{K,li}\cdot F_{K,lj}\cdot X_i^{el}(t)\cdot \dot{X}_j^{el}(t)\right)\cdot \Delta k_l. \tag{16}$$

The corresponding control law, aiming at minimizing the elastic energy, is

$$\begin{cases} \Delta k_l = \max(\Delta k_l) & \text{if } \sum_{i=1}^{n}\sum_{j=1}^{n} B_{K,li}\cdot F_{K,lj}\cdot X_i^{el}(t)\cdot \dot{X}_j^{el}(t) < 0, \\ \Delta k_l = \min(\Delta k_l) & \text{if } \sum_{i=1}^{n}\sum_{j=1}^{n} B_{K,li}\cdot F_{K,lj}\cdot X_i^{el}(t)\cdot \dot{X}_j^{el}(t) > 0. \end{cases} \tag{17}$$

In contrast to the total displacement, which is obtained directly by integrating the equation of motion, in the FAM approach the elastic component of the displacement is reconstructed based on the plastic rotations of the hinges. This makes it appropriate to reformulate the control algorithm conditions in terms of these two quantities. Specifically, using Equation (3), it can be written as follows:

$$X_i^{el}(t) = X_i(t) - X_i^{inel}(t) = X_i(t) - \sum_{k=1}^{n}\sum_{l=1}^{m} K_{ik}^{-1}\cdot K_{P,kl}\cdot \theta_l^{inel}(t), \tag{18}$$

thus during the evaluation, the product of the dynamic terms present in Equation (17) should be formally assessed as follows:

$$\begin{aligned} X_i^{el}(t)\cdot \dot{X}_j^{el}(t) &= \left(X_i(t) - \sum_{k=1}^{n}\sum_{l=1}^{m} K_{ik}^{-1}\cdot K_{P,kl}\cdot \theta_l^{inel}(t)\right) \\ &\quad \cdot\left(\dot{X}_j(t) - \sum_{k=1}^{n}\sum_{l=1}^{m} K_{jk}^{-1}\cdot K_{P,kl}\cdot \dot{\theta}_l^{inel}(t)\right) \\ &= X_i(t)\cdot \dot{X}_j(t) - X_i(t)\cdot \sum_{k=1}^{n}\sum_{l=1}^{m} K_{jk}^{-1}\cdot K_{P,kl}\cdot \dot{\theta}_l^{inel}(t) - \dot{X}_j(t) \\ &\quad \cdot \sum_{k=1}^{n}\sum_{l=1}^{m} K_{ik}^{-1}\cdot K_{P,kl}\cdot \theta_l^{inel}(t) + \sum_{q=1}^{m}\sum_{l=1}^{m} \theta_l^{inel}(t)\cdot \dot{\theta}_q^{inel}(t) \\ &\quad \cdot\left(\sum_{k=1}^{n} K_{ik}^{-1}\cdot K_{P,kl}\right)\cdot\left(\sum_{p=1}^{n} K_{jp}^{-1}\cdot K_{P,pq}\right). \end{aligned} \tag{19}$$

3.3 | Minimization of Hysteretic Dissipated Power

Applying the same derivation steps, the hysteretic power term, $P_{hys}(K_{tot}) = X^{el\,T}(t)\cdot K_{tot}\cdot(t)\cdot \dot{X}^{inel}$, can be expressed in terms of the controllable stiffness contributions, leading to

$$\begin{aligned} P_{hys}(K_{tot}) &= \sum_{i=1}^{n}\sum_{j=1}^{n} K_{ij}\cdot X_i^{el}(t)\cdot \dot{X}_j^{inel}(t) + \sum_{l=1}^{r} k_l \\ &\quad \cdot\left(\sum_{i=1}^{n}\sum_{j=1}^{n} B_{K,li}\cdot F_{K,lj}\cdot X_i^{el}(t)\cdot \dot{X}_j^{inel}(t)\right). \end{aligned} \tag{20}$$

The sensitivity equation can be thus written as in the following:

$$\Delta P_{hys,l} = \frac{\partial P_{hys}}{\partial k_l}\cdot \Delta k_l = \left(\sum_{i=1}^{n}\sum_{j=1}^{n} B_{K,li}\cdot F_{K,lj}\cdot X_i^{el}(t)\cdot \dot{X}_j^{inel}(t)\right)\Delta k_l, \tag{21}$$

which leads to the corresponding control law aiming at minimizing the hysteretic energy:

$$\begin{cases} \Delta k_l = \max(\Delta k_l) & \text{if } \sum_{i=1}^{n}\sum_{j=1}^{n} B_{K,li}\cdot F_{K,lj}\cdot X_i^{el}(t)\cdot \dot{X}_j^{inel}(t) < 0, \\ \Delta k_l = \min(\Delta k_l) & \text{if } \sum_{i=1}^{n}\sum_{j=1}^{n} B_{K,li}\cdot F_{K,lj}\cdot X_i^{el}(t)\cdot \dot{X}_j^{inel}(t) > 0. \end{cases} \tag{22}$$

scihm, 2026, 1, Downloaded from https://onlinelibrary.wiley.com/doi/10.1155/stc/8260623 by M. De Iuliis - Politecnico Di Torino Sist. Bibl Del Polit Di Torino , Wiley Online Library on [13/08/2026]. See the Terms and Conditions (https://onlinelibrary.wiley.com/terms-and-conditions) on Wiley Online Library for rules of use; OA articles are governed by the applicable Creative Commons License

whereas the product of the two dynamic terms in the control law can be also usefully reformulated as follows:

$$\mathrm{X}_i^{el}(t)\cdot\dot{\mathrm{X}}_j^{inel}(t)=\mathrm{X}_i(t)\cdot\sum_{k=1}^{n}\sum_{l=1}^{m}\mathrm{K}_{j,k}^{-1}\cdot\mathrm{K}_{P,kl}\cdot\dot{\theta}_l^{inel}(t)+\sum_{q=1}^{m}\sum_{l=1}^{m}\theta_l^{inel}(t)\cdot\dot{\theta}_q^{inel}(t)\cdot\left(\sum_{k=1}^{n}\mathrm{K}_{i,k}^{-1}\cdot\mathrm{K}_{P,kl}\right)\cdot\left(\sum_{p=1}^{n}\mathrm{K}_{j,p}^{-1}\cdot\mathrm{K}_{P,pq}\right). \tag{23}$$

3.4 | Minimization of Kinetic Energy

Although the kinetic power does not explicitly depend on stiffness and damping, it can be reformulated using the equation of motion. This allows expressing the dependence on the controllable mechanical properties as follows:

$$\begin{aligned}P_K(\mathrm{C}_{tot},\mathrm{K}_{tot})=&-\sum_{l=1}^{s}\mathrm{c}_l\cdot\left(\sum_{i=1}^{n}\sum_{j=1}^{n}\mathrm{B}_{C,li}\cdot\mathrm{F}_{C,lj}\cdot\dot{\mathrm{X}}_i(t)\cdot\dot{\mathrm{X}}_j(t)\right)\\&-\sum_{i=1}^{n}\sum_{j=1}^{n}\mathrm{K}_{ij}\cdot\mathrm{X}_i^{el}(t)\cdot\dot{\mathrm{X}}_j(t)-\sum_{l=1}^{r}k_l\\&\cdot\left(\sum_{i=1}^{n}\sum_{j=1}^{n}\mathrm{B}_{K,li}\cdot\mathrm{F}_{K,lj}\cdot\mathrm{X}_i^{el}(t)\cdot\dot{\mathrm{X}}_j(t)\right)\\&-\sum_{i=1}^{n}\sum_{j=1}^{n}\mathrm{M}_{ij}\cdot\ddot{\mathrm{U}}_{g,i}(t)\cdot\dot{\mathrm{X}}_j(t),\end{aligned} \tag{24}$$

and deriving the corresponding sensitivities as follows:

$$\begin{aligned}\Delta P_{K,l}&=\left(\frac{\partial P_K}{\partial c_l}\right)\cdot\Delta c_l+\left(\frac{\partial P_K}{\partial k_l}\right)\cdot\Delta\mathrm{k}_l\\&=-\left(\sum_{i=1}^{n}\sum_{j=1}^{n}\mathrm{B}_{C,li}\cdot\mathrm{F}_{C,lj}\cdot\dot{\mathrm{X}}_i(t)\cdot\dot{\mathrm{X}}_j(t)\right)\cdot\Delta c_l\\&\quad-\left(\sum_{i=1}^{n}\sum_{j=1}^{n}\mathrm{B}_{K,li}\cdot\mathrm{F}_{K,lj}\cdot\mathrm{X}_i^{el}(t)\cdot\dot{\mathrm{X}}_j(t)\right)\cdot\Delta\mathrm{k}_l,\end{aligned} \tag{25}$$

and with the aim of minimizing this term, the following control laws can be defined:

$$\begin{cases}\Delta\mathrm{c}_l=\max(\Delta\mathrm{c}_l) & \text{if }\sum_{i=1}^{n}\sum_{j=1}^{n}\mathrm{B}_{C,li}\cdot\mathrm{F}_{C,lj}\cdot\dot{\mathrm{X}}_i(t)\cdot\dot{\mathrm{X}}_j(t)>0,\\ \Delta\mathrm{c}_l=\min(\Delta\mathrm{c}_l) & \text{if }\sum_{i=1}^{n}\sum_{j=1}^{n}\mathrm{B}_{C,li}\cdot\mathrm{F}_{C,lj}\cdot\dot{\mathrm{X}}_i(t)\cdot\dot{\mathrm{X}}_j(t)<0.\end{cases} \tag{26}$$

$$\begin{cases}\Delta\mathrm{k}_l=\max(\Delta\mathrm{k}_l) & \text{if }\sum_{i=1}^{n}\sum_{j=1}^{n}\mathrm{B}_{K,li}\cdot\mathrm{F}_{K,lj}\cdot\mathrm{X}_i^{el}(t)\cdot\dot{\mathrm{X}}_j(t)>0,\\ \Delta\mathrm{k}_l=\min(\Delta\mathrm{k}_l) & \text{if }\sum_{i=1}^{n}\sum_{j=1}^{n}\mathrm{B}_{K,li}\cdot\mathrm{F}_{K,lj}\cdot\mathrm{X}_i^{el}(t)\cdot\dot{\mathrm{X}}_j(t)<0.\end{cases} \tag{27}$$

The control law (27) can be conveniently reformulated in terms of total and inelastic displacements as follows:

$$\mathrm{X}_i^{el}(t)\cdot\dot{\mathrm{X}}_j(t)=\mathrm{X}_i(t)\cdot\dot{\mathrm{X}}_j(t)-\left(\sum_{k=1}^{n}\sum_{l=1}^{m}\mathrm{K}_{i,k}^{-1}\cdot\mathrm{K}_{P,kl}\cdot\theta_l^{inel}(t)\right)\cdot\dot{\mathrm{X}}_j(t). \tag{28}$$

3.5 | Minimization of the Input Energy

Similarly, the input power can be reformulated using the equation of motion, allowing its dependence on the controllable parameters to be made explicit as follows:

$$\begin{aligned}P_{in}(\mathrm{C},\mathrm{K})=&\sum_{i=1}^{n}\sum_{j=1}^{n}\mathrm{M}_{ij}\cdot\ddot{\mathrm{X}}_i(t)\cdot\dot{\mathrm{X}}_j(t)+\sum_{i=1}^{n}\sum_{j=1}^{n}\mathrm{C}_{ij}\cdot\dot{\mathrm{X}}_i(t)\cdot\dot{\mathrm{X}}_j(t)+\sum_{l=1}^{s}\mathrm{c}_l\\&\cdot\left(\sum_{i=1}^{n}\sum_{j=1}^{n}\mathrm{B}_{C,li}\cdot\mathrm{F}_{C,lj}\cdot\dot{\mathrm{X}}_i(t)\cdot\dot{\mathrm{X}}_j(t)\right)+\sum_{i=1}^{n}\sum_{j=1}^{n}\mathrm{K}_{ij}\cdot\mathrm{X}_i^{el}(t)\cdot\dot{\mathrm{X}}_j(t)\\&+\sum_{l=1}^{r}k_l\cdot\left(\sum_{i=1}^{n}\sum_{j=1}^{n}\mathrm{B}_{K,li}\cdot\mathrm{F}_{K,lj}\cdot\mathrm{X}_i^{el}(t)\cdot\dot{\mathrm{X}}_j(t)\right),\end{aligned} \tag{29}$$

yielding the variation of this quantity with respect to stiffness and damping as follows:

$$\begin{aligned}\Delta P_{in,l}&=\left(\frac{\partial P_K}{\partial c_l}\right)\cdot\Delta c_l+\left(\frac{\partial P_K}{\partial k_l}\right)\cdot\Delta\mathrm{k}_l\\&=\left(\sum_{i=1}^{n}\sum_{j=1}^{n}\mathrm{B}_{C,li}\cdot\mathrm{F}_{C,lj}\cdot\dot{\mathrm{X}}_i(t)\cdot\dot{\mathrm{X}}_j(t)\right)\cdot\Delta c_l\\&\quad+\left(\sum_{i=1}^{n}\sum_{j=1}^{n}\mathrm{B}_{K,li}\cdot\mathrm{F}_{K,lj}\cdot\mathrm{X}_i^{el}(t)\cdot\dot{\mathrm{X}}_j(t)\right)\cdot\Delta\mathrm{k}_l,\end{aligned} \tag{30}$$

and to the definition of the following control laws:

$$\begin{cases}\Delta\mathrm{c}_l=\max(\Delta\mathrm{c}_l) & \text{if }\sum_{i=1}^{n}\sum_{j=1}^{n}\mathrm{B}_{C,li}\cdot\mathrm{F}_{C,lj}\cdot\dot{\mathrm{X}}_i(t)\cdot\dot{\mathrm{X}}_j(t)<0,\\ \Delta\mathrm{c}_l=\min(\Delta\mathrm{c}_l) & \text{if }\sum_{i=1}^{n}\sum_{j=1}^{n}\mathrm{B}_{C,li}\cdot\mathrm{F}_{C,lj}\cdot\dot{\mathrm{X}}_i(t)\cdot\dot{\mathrm{X}}_j(t)>0.\end{cases} \tag{31}$$

$$\begin{cases}\Delta\mathrm{k}_l=\max(\Delta\mathrm{k}_l) & \text{if }\sum_{i=1}^{n}\sum_{j=1}^{n}\mathrm{B}_{K,li}\cdot\mathrm{F}_{K,lj}\cdot\mathrm{X}_i^{el}(t)\cdot\dot{\mathrm{X}}_j(t)<0,\\ \Delta\mathrm{k}_l=\min(\Delta\mathrm{k}_l) & \text{if }\sum_{i=1}^{n}\sum_{j=1}^{n}\mathrm{B}_{K,li}\cdot\mathrm{F}_{K,lj}\cdot\mathrm{X}_i^{el}(t)\cdot\dot{\mathrm{X}}_j(t)>0.\end{cases} \tag{32}$$

with the product in Equation (32), which can be reformulated as previously shown in Equation (28).

It can be observed that the last two control strategies lead to perfectly complementary laws, as a consequence of their fundamentally different physical objectives. The minimization of input power aims to reduce the transfer of energy from the ground motion to the structure by minimizing the relative velocities at the base, effectively promoting the motion of the structure in phase with the seismic excitation. Conversely, the minimization of kinetic energy seeks to reduce the absolute velocities of the system, requiring maximum dissipation when the velocities are high and thus favoring isolation from the ground motion. These objectives are inherently contradictory: the first strategy promotes dynamic coupling with the base, while the second promotes dynamic decoupling. Consequently, the conditions that are favorable for one criterion, such as the motion of the structure being in phase with the ground displacement, are precisely those that are unfavorable for the other, resulting in

scihn, 2026, 1, Downloaded from https://onlinelibrary.wiley.com/doi/10.1155/stc/8260623 by M. De Iuliis - Politecnico Di Torino Sist. Bibl Del Polit Di Torino , Wiley Online Library on [13/08/2026]. See the Terms and Conditions (https://onlinelibrary.wiley.com/terms-and-conditions) on Wiley Online Library for rules of use; OA articles are governed by the applicable Creative Commons License

TABLE 1 | Semiactive control laws for the different considered algorithms.

Objective of the algorithm	Extrastructural damping	Extrastructural stiffness
Maximization of dissipated energy	$\begin{cases} \Delta c_l \geq 0 & \text{if } \sum_{i=1}^{n}\sum_{j=1}^{n} B_{C,li} \cdot F_{C,lj} \cdot \dot{X}_i(t) \cdot \dot{X}_j(t) \geq 0 \\ \Delta c_l < 0 & \text{if } \sum_{i=1}^{n}\sum_{j=1}^{n} B_{C,li} \cdot F_{C,lj} \cdot \dot{X}_i(t) \cdot \dot{X}_j(t) < 0 \end{cases}$	No control
Minimization of elastic energy	No control	$\begin{cases} \Delta k_l \geq 0 & \text{if } \sum_{i=1}^{n}\sum_{j=1}^{n} B_{K,li} \cdot F_{K,lj} \cdot X_i^{el}(t) \cdot \dot{X}_j^{el}(t) < 0 \\ \Delta k_l < 0 & \text{if } \sum_{i=1}^{n}\sum_{j=1}^{n} B_{K,li} \cdot F_{K,lj} \cdot X_i^{el}(t) \cdot \dot{X}_j^{el}(t) > 0 \end{cases}$
Minimization of hysteretic energy	No control	$\begin{cases} \Delta k_l \geq 0 & \text{if } \sum_{i=1}^{n}\sum_{j=1}^{n} B_{K,li} \cdot F_{K,lj} \cdot X_i^{el}(t) \cdot \dot{X}_j^{inel}(t) < 0 \\ \Delta k_l < 0 & \text{if } \sum_{i=1}^{n}\sum_{j=1}^{n} B_{K,li} \cdot F_{K,lj} \cdot X_i^{el}(t) \cdot \dot{X}_j^{inel}(t) > 0 \end{cases}$
Minimization of kinetic energy	$\begin{cases} \Delta c_l \geq 0 & \text{if } \sum_{i=1}^{n}\sum_{j=1}^{n} B_{C,li} \cdot F_{C,lj} \cdot \dot{X}_i(t) \cdot \dot{X}_j(t) \geq 0 \\ \Delta c_l < 0 & \text{if } \sum_{i=1}^{n}\sum_{j=1}^{n} B_{C,li} \cdot F_{C,lj} \cdot \dot{X}_i(t) \cdot \dot{X}_j(t) < 0 \end{cases}$	$\begin{cases} \Delta k_l \geq 0 & \text{if } \sum_{i=1}^{n}\sum_{j=1}^{n} B_{K,li} \cdot F_{K,lj} \cdot X_i^{el}(t) \cdot \dot{X}_j(t) \geq 0 \\ \Delta k_l < 0 & \text{if } \sum_{i=1}^{n}\sum_{j=1}^{n} B_{K,li} \cdot F_{K,lj} \cdot X_i^{el}(t) \cdot \dot{X}_j(t) < 0 \end{cases}$
Minimization of input energy	$\begin{cases} \Delta c_l \geq 0 & \text{if } \sum_{i=1}^{n}\sum_{j=1}^{n} B_{C,li} \cdot F_{C,lj} \cdot \dot{X}_i(t) \cdot \dot{X}_j(t) \leq 0 \\ \Delta c_l < 0 & \text{if } \sum_{i=1}^{n}\sum_{j=1}^{n} B_{C,li} \cdot F_{C,lj} \cdot \dot{X}_i(t) \cdot \dot{X}_j(t) > 0 \end{cases}$	$\begin{cases} \Delta k_l \geq 0 & \text{if } \sum_{i=1}^{n}\sum_{j=1}^{n} B_{K,li} \cdot F_{K,lj} \cdot X_i^{el}(t) \cdot \dot{X}_j(t) \leq 0 \\ \Delta k_l < 0 & \text{if } \sum_{i=1}^{n}\sum_{j=1}^{n} B_{K,li} \cdot F_{K,lj} \cdot X_i^{el}(t) \cdot \dot{X}_j(t) > 0 \end{cases}$

complementary switching logics. This dichotomy reflects the classical trade-off in structural control between reducing base forces (minimization of input power) and reducing displacements/velocities in the superstructure (minimization of kinetic energy).

For the sake of clarity, the laws identified for the considered algorithms are summarized in Table 1, where the variations in both damping and stiffness properties of the semiactive devices are shown.

It is relevant to underline how the proposed control framework is expected to behave in the presence of typical sources of uncertainty, including measurement noise as well as uncertainties arising from sensors and actuators. These effects can affect the evaluation of the state variables entering the control laws; however, the adopted switching logic depends only on the sign of scalar sensitivity terms, making it inherently robust when these quantities are sufficiently far from zero. Close to the switching conditions, where noise or other uncertainties arising from sensor/actuator dynamics and parameter variability may induce undesired rapid switching (chattering), standard remedies such as the introduction of a small dead-band, low-pass filtering, or conservative threshold selection can be effectively employed without altering the overall control logic. Moreover, in a real implementation, plastic rotations are not directly measurable but can be reconstructed from relative displacement measurements close to the beam-column nodes, a task that is technically feasible with current sensing technologies but requires a dedicated instrumentation strategy.

4 | Description of the Benchmark Structures and Seismic Excitations Considered

In the present work, the numerical analyses aimed at evaluating the performance of the proposed semiactive control algorithms are carried out with reference to two benchmark structural systems, briefly described in Sections 4.1 and 4.2, and 85 seismic excitations characterized by different dynamic properties, as described in Section 4.3. The reference structural systems belong to the SAC Project for the Los Angeles (California) region, whose objective was to provide a common basis for evaluating the performance of various control systems [46, 50]. In particular, the benchmarks proposed for nonlinear response analysis were designed in accordance with the seismic design codes in force in the United States at the time of the initiation of the SAC project (early 2000 s) and represent two structural typologies: low-rise and medium-rise buildings commonly used in seismic regions.

In order to properly represent the nonlinear behavior of the systems during seismic events, the considered structures were modeled using an elastic–perfectly plastic hysteresis model at the ends of the structural elements (plastic hinges), a choice that, despite its simplicity, makes it possible to effectively capture the mechanisms of plastic hinge formation and the resulting redistribution of internal forces. The use of an elastic–perfectly plastic model implies that the accuracy of the response may depend on the level of idealization adopted for the constitutive behavior. Nevertheless, such simplified models are commonly used in control-oriented formulations, as they help to limit the uncertainty associated with parameters that are difficult to

scihm, 2026, 1, Downloaded from https://onlinelibrary.wiley.com/doi/10.1155/stc/8260623 by M. De Iuliis - Politecnico Di Torino Sist. Bibl Del Polit Di Torino , Wiley Online Library on [18/08/2026]. See the Terms and Conditions (https://onlinelibrary.wiley.com/terms-and-conditions) on Wiley Online Library for rules of use; OA articles are governed by the applicable Creative Commons License

calibrate, while providing a robust representation of the structure's seismic response in terms of all relevant energy components. This modeling approach is, therefore, well suited to the analyses carried out in the present work, where the primary objective is to assess the effectiveness of the proposed control algorithms under conditions that remain clear and readily interpretable.

4.1 | Three-Story Benchmark Building (BS1)

The BS1 structure has plan dimensions of $36.58\,m \times 54.87\,m$, with a total height of $11.89\,m$. The lateral-load-resisting system consists of steel MRF perimeter frames, with a bay spacing of $9.15\,m$ in both directions. The columns are made of steel with a yield stress of $345\,MPa$, while the beams are wide-flange profiles with a yield stress of $248\,MPa$. The floors are steel–concrete composite slabs, assumed to be rigid in the horizontal plane to ensure diaphragm action. The typical story height is $3.96\,m$. The column bases are considered fixed to the ground. The total seismic mass of the structure is $2.95 \times 10^6\,kg$, distributed over the three aboveground levels. The first three natural frequencies of the system are $0.99\,Hz$, $3.06\,Hz$, and $5.83\,Hz$, characteristics typical of a relatively stiff, low-rise structure (Figure 1).

4.2 | Nine-Story Benchmark Building (BS2)

The BS2 structure has a square plan of $45.73\,m \times 45.73\,m$ and a total height of $37.19\,m$. In this case as well, the lateral-load-resisting system consists of steel moment-resisting perimeter frames with a bay spacing of $9.15\,m$. The structure includes one basement level (B-1) and nine aboveground levels. The columns employ a "two-tier" construction, i.e., monolithic elements connected every two stories starting from the first floor, with seismic joints located $1.83\,m$ above the beam–column nodes. The column bases are modeled as pinned at the B-1 level, while concrete foundation walls and the surrounding soil prevent horizontal displacements at ground level. The typical story height is $3.96\,m$, except for the basement ($3.65\,m$) and the first aboveground level ($5.49\,m$). The total seismic mass of the aboveground levels is $9.00 \times 10^6\,kg$. The first five natural frequencies are $0.443\,Hz$, $1.18\,Hz$, $2.05\,Hz$, $3.09\,Hz$, and $4.27\,Hz$, reflecting greater flexibility compared to the three-story building (Figure 2).

4.3 | Considered Recorded Ground Motions

A total of 85 natural seismic records was selected for the numerical investigation, with Tables 2 and 3 summarizing their main properties. These events, chosen for their highly variable characteristics, can be classified into two main groups [51]: 45 FF seismic inputs and 40 NF seismic inputs. Each seismic input is identified by a numerical label, from 1 to 85, which will be used for reference throughout.

In particular, the FF recordings are further subdivided into three subsets based on the PGA/PGV ratio [41]: high ratio (HR), labels 1–15; medium ratio (MR), labels 16–30; and low ratio (LR), labels 31–45, whereas the NF recordings (labels 46–85) exhibit markedly higher specific energy density (SED), with energy concentrated in the low-frequency range, reflecting the strong energy content and impulsive, pulse-type features that characterize near-source ground motions [52, 53] (Figure 3).

These indices used to characterize the seismic excitations have significant physical meanings: the PGA/PGV ratio is a very effective parameter for providing information on the frequency content and duration of ground motions [54, 55]; the SED captures the impulsive nature and the energy concentration of seismic events and contains the largest amount of information related to the structural response according to the Shannon entropy metric [56, 57].

The ground motions considered are all recorded events corresponding to high return periods with highly variable seismic demands and dynamic properties. Since the main objective of the present paper is to assess the effectiveness of the different control algorithms under conditions where the considered structures exhibit nonlinear behavior, it was necessary to scale the intensity of the recorded accelerograms. Specifically, for the three-story benchmark building, a target spectral pseudoacceleration corresponding to the first modal period was set to 0.1 g (Figure 4a), whereas for the nine-story benchmark building, considering the longer vibration period associated with its first mode, the corresponding value was set to 0.05 g (Figure 4b). This choice, which is compatible with a wide range of PGA values, induces nonlinear dynamic behavior in the analyzed structures for all considered seismic events, with plastic excursions of varying intensity: some events lead to the formation of only a few isolated plastic hinges with negligible residual deformations, while others result in

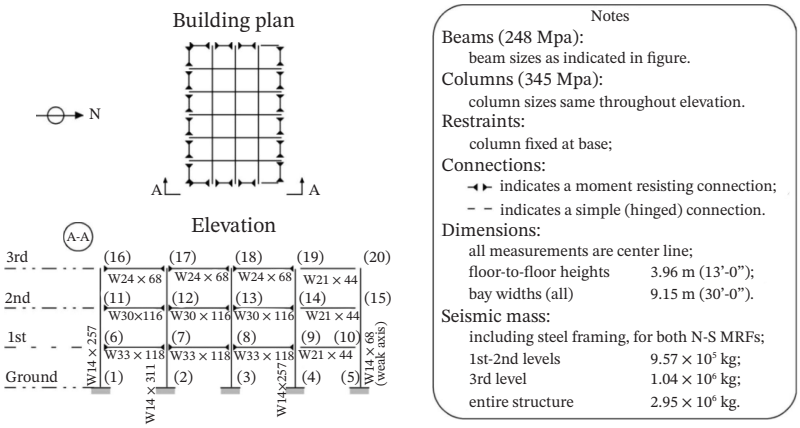

FIGURE 1 | Three-story benchmark building north–south moment-resisting frame (from [46]).

sdhm, 2026, 1, Downloaded from https://onlinelibrary.wiley.com/doi/10.1155/stc/8260623 by M. De Iuliis - Politecnico Di Torino Sist. Bibl Del Polit Di Torino , Wiley Online Library on [13/08/2026]. See the Terms and Conditions (https://onlinelibrary.wiley.com/terms-and-conditions) on Wiley Online Library for rules of use; OA articles are governed by the applicable Creative Commons License

widespread plasticization and structures approaching collapse, providing an opportunity to test the proposed algorithms under general and realistic conditions.

4.4 | Validation of the FAM-Based Numerical Model

To validate the FAM-based equation of motion adopted in this study, a specific analysis has been carried out by comparing the dynamic response obtained through the proposed implementation against the results of independent nonlinear time-history analyses performed in SAP2000 [58].

The FAM-based model was implemented in MATLAB [59] through the explicit assembly of the characteristic matrices of the method, namely the global stiffness matrix K, the plastic hinge connectivity matrix K_P, and the plastic hinge stiffness matrix K_R, based on the geometric and mechanical properties of the benchmark structures. At each time step, the plastic rotations at the potential hinge locations were evaluated by solving the characteristic equation of the method, Equation (1), together with the constitutive relationship of the plastic hinges. The equation of motion (4) was then integrated using the built-in MATLAB ODE solver [60]. The SAP2000 model was constructed to reproduce the same nonlinear description adopted in the FAM framework, employing concentrated plastic hinges with an elastic–perfectly plastic moment–rotation relationship and the same proportional damping formulation. The dynamic analyses in SAP2000 were performed using the Hilber–Hughes–Taylor (HHT) implicit integration algorithm [61].

The validation was carried out on both benchmark structures, BS1 and BS2, under the full set of 85 considered seismic excitations. For illustrative purposes, the comparison between the two models is presented in Figures 5–8 in terms of absolute floor displacement time histories at all story levels, with reference to two selected ground motion records chosen as representative of the most demanding excitation conditions within the dataset: record #14 of the FF set, characterized by the highest PGA/PGV ratio, and record #76 of the NF set, characterized by the highest SED. Specifically, Figure 5a shows the dynamic response of benchmark BS1 to seismic excitation #14 in the case of the FAM model, whereas Figure 5b shows the same response modeled using SAP2000. Figure 6 refers to the same two cases for seismic event #76, while Figures 7–8 are analogous to the previous two, but refer to structural system BS2. Additionally, the plastic rotation time histories at selected potential hinge locations have been considered to verify the consistency of the inelastic response.

The results show a very close agreement between the two models across all considered seismic excitations, with differences in peak displacement values and maximum plastic rotations of the order of a few percentage points. These discrepancies are consistent with those reported in the literature for FAM-based implementations validated against commercial software and refined finite element models [34, 62, 63] and are attributable to the different numerical integration schemes employed. Overall, the validation confirms the reliability and accuracy of the proposed FAM-based formulation as a basis for the derivation and implementation

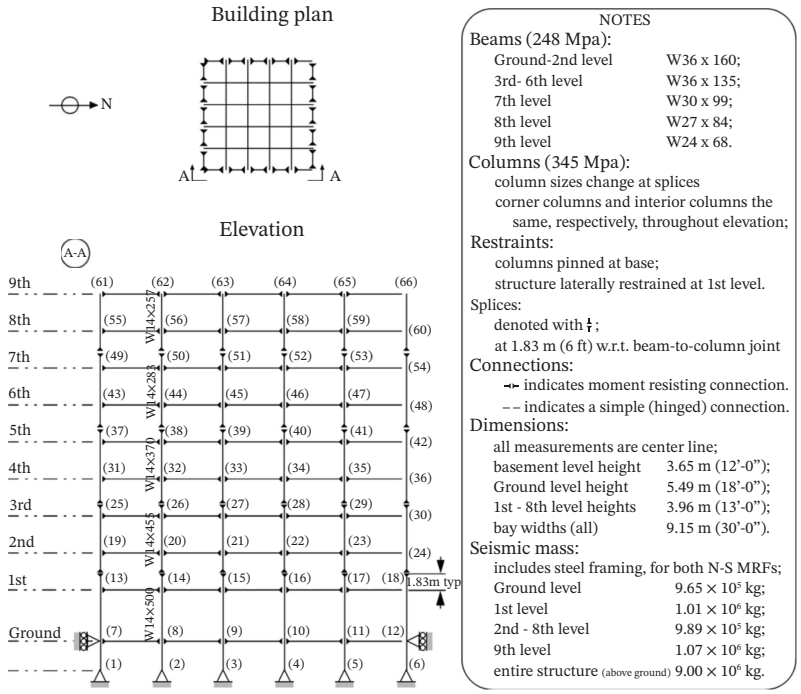

FIGURE 2 | Nine-story benchmark building north–south moment-resisting frame (from [46]).

scihm, 2026, 1, Downloaded from https://onlinelibrary.wiley.com/doi/10.1155/stc/8260623 by M. De Iuliis - Politecnico Di Torino Sist. Bibl Del Polit Di Torino , Wiley Online Library on [18/08/2026]. See the Terms and Conditions (https://onlinelibrary.wiley.com/terms-and-conditions) on Wiley Online Library for rules of use; OA articles are governed by the applicable Creative Commons License

TABLE 2 | Considered far-field seismic records.

#	Earthquake	Date	Mg	PGA (m/sec^2)	Site	Epic. Dist. (km)	Comp.	PGA/ PGV (sec^{-1})	Specific energy density (m^2/sec)	Soil (EC 8 class.)
1	Parkfield, California	June 27, 1966	5.6	2.594	Temblor No. 2	7	N65W	18.87	0.0172	A
2	Parkfield, California	June 27, 1966	5.6	4.176	Cholame, Shandon No. 5	5	N85W	16.39	0.0622	A
3	San Francisco, California	Mar. 22, 1957	5.2	1.009	Golden Gate Park	11	S80E	25.00	0.0012	A
4	San Francisco, California	Mar. 22, 1957	5.2	0.823	State Bldg., S.F.	17	S09E	20.83	0.0022	B
5	Helena, Montana	Oct. 31, 1935	6	1.410	Carroll College	8	N00E	19.61	0.0022	A
6	Lytle Creek	Sep. 12, 1970	5.4	1.910	Wrightwood, California	15	S25W	18.87	0.0032	A
7	Oroville, California	Aug. 1, 1975	5.7	0.807	Seismogr. Station, Oroville	13	N53W	16.39	0.0012	A
8	San Fernando, California	Feb. 9, 1971	6.4	10.350	Pacomia Dam	4	S74W	17.86	0.3092	A
9	San Fernando, California	Feb. 9, 1971	6.4	1.407	Lake Hughes, Station 4	26	S21W	16.67	0.0062	A
10	Nahanni N.W.T., Canada	Dec. 23, 1985	6.9	10.610	Site 1, Iverson	7.5	LONG	23.26	0.1342	A
11	Central Honshu, Japan	Feb. 26, 1971	5.5	1.453	Yoneyama Bridge	27	TRANS	25.00	0.0012	B
12	Near E. Coast of Honshu, Japan	May. 11, 1972	5.8	1.401	Kushiro Central Wharf	33	N00E	24.39	0.0032	B
13	Honshu, Japan	Apr. 5, 1966	5.4	2.604	Hoshina–A	4	N00E	22.73	0.0032	B
14	Monte Negro, Yugoslavia	Apr. 9, 1979	5.4	0.405	Albatros Hotel, Ulcinj	12.5	N00E	25.64	0.0002	A
15	Banja Luka, Yugoslavia	Aug. 13, 1981	6.1	0.709	Seism. Station, Banja Luka	8.5	N90W	22.73	0.0012	A
16	Imperial Valley, California	May 18, 1940	6.6	3.348	El Centro	8	S00E	9.26	0.2132	B
17	Kern County, California	July 21, 1952	7.6	1.727	Taft Lincoln School Tunnel	56	S69E	10.42	0.0982	A
18	Kern County, California	July 21, 1952	7.6	1.500	Taft Lincoln School Tunnel	56	N21E	9.01	0.0782	A
19	Borrego Mtn., California	April 8, 1968	6.5	0.446	San Onofre SCE Power Plant	122	N57W	10.87	0.0082	B
20	Borrego Mtn., California	April 8, 1968	6.5	0.393	San Onofre SCE Power Plant	122	N33E	10.99	0.0042	B
21	San Fernando, California	Feb. 9, 1971	6.4	1.448	3838 Lankershim Blvd., L.A.	24	S90W	9.35	0.0272	A
22	San Fernando, California	Feb. 9, 1971	6.4	2.031	Hollywood Storage P.E. Lot, L.A.	35	N90E	10.10	0.1322	B
23	San Fernando, California	Feb. 9, 1971	6.4	1.590	3407 6th Street, L.A.	39	N90E	10.10	0.0772	B
24	San Fernando, California	Feb. 9, 1971	6.4	1.735	Griffith Park Observatory, L.A.	31	S00W	8.47	0.0502	A
25	San Fernando, California	Feb. 9, 1971	6.4	1.920	234 Figueroa St., L.A.	41	N37E	11.90	0.0662	B
26	Near E. Coast of Honshu, Japan	Nov. 16, 1974	6.1	0.677	Kashima Harbor Works	38	N00E	9.43	0.0052	B
27	Near E. Coast of Honshu, Japan	Aug. 2, 1971	7	0.746	Kushiro Central Wharf	196	N90E	10.99	0.0092	B
28	Monte Negro, Yugoslavia	Apr. 15, 1979	7	1.650	Albatros Hotel, Ulcinj	17	N00E	8.40	0.0502	A
29	Mexico Earthquake	Sept. 19 1985	8.1	1.012	El Suchil, Guerrero Array	230	S00E	8.85	0.0172	A
30	Mexico Earthquake	Sept. 19 1985	8.1	1.185	La Villita, Guerrero Array	44	N90E	11.63	0.0272	A
31	Long Beach, California	Mar. 10, 1933	6.3	0.938	Subway Terminal, L.A.	59	N51W	4.22	0.1752	A

(Continues)

scm, 2026, 1, Downloaded from https://onlinelibrary.wiley.com/doi/10.1155/stc/8260623 by M. De Iuliis - Politecnico Di Torino Sist. Bibl Del Polit Di Torino , Wiley Online Library on [18/08/2026]. See the Terms and Conditions (https://onlinelibrary.wiley.com/terms-and-conditions) on Wiley Online Library for rules of use; OA articles are governed by the applicable Creative Commons License

TABLE 2 | (Continued)

#	Earthquake	Date	Mg	PGA (m/sec^2)	Site	Epic. Dist. (km)	Comp.	PGA/ PGV (sec^{-1})	Specific energy density (m^2/sec)	Soil (EC 8 class.)
32	Long Beach, California	Mar. 10, 1933	6.3	0.612	Subway Terminal, L.A.	59	N39E	3.61	0.0922	A
33	Lower California	Dec. 30, 1934	6.5	1.538	El Centro	58	S00W	7.04	0.0412	B
34	San Fernando, California	Feb. 9, 1971	6.4	0.968	2500 Wilshire Blvd., L.A.	40	N61W	5.13	0.0542	B
35	San Fernando, California	Feb. 9, 1971	6.4	1.273	3550 Wilshire Blvd., L.A.	39	WEST	6.06	0.0882	B
36	San Fernando, California	Feb. 9, 1971	6.4	1.245	222 Figueroa St., L.A.	41	S37W	6.76	0.0622	B
37	San Fernando, California	Feb. 9, 1971	6.4	1.098	3470 Wilshire Blvd., L.A.	39	S90W	6.21	0.1072	B
38	San Fernando, California	Feb. 9, 1971	6.4	1.131	4680 Wilshire Blvd., L.A.	38	N15E	5.35	0.0912	B
39	San Fernando, California	Feb. 9, 1971	6.4	1.148	445 Figueroa St., L.A.	41	S38W	6.62	0.0692	A
40	San Fernando, California	Feb. 9, 1971	6.4	1.018	Hollywood Storage L.A.	32	S00W	6.33	0.0532	B
41	Near E. Coast of Honshu, Japan	May 16, 1968	7.9	2.173	Muroran Harbor	290	N00E	6.67	0.0842	B
42	Near E. Coast of Honshu, Japan	June 17, 1973	7.4	1.971	Kushiro Central Wharf	112	N00E	6.80	0.1662	B
43	Mexico Earthquake	Sep. 19, 1985	8.1	0.994	Zihuatenejo, Guerrero Array	135	S00E	6.41	0.0622	A
44	Mexico Earthquake	Sep. 19, 1985	8.1	0.501	Teacalco, Cuerrero Array	333	N00E	5.99	0.0272	A
45	Mexico Earthquake	Sep. 19, 1985	8.1	0.381	Mesa Vibradora C.U., Mexico City	379	N90W	3.66	0.0362	A

scim, 2026, 1, Downloaded from https://onlinelibrary.wiley.com/doi/10.1155/sc/8260623 by M. De Iuliis - Politecnico Di Torino Sist. Bibl Del Polit Di Torino , Wiley Online Library on [18/08/2026]. See the Terms and Conditions (https://onlinelibrary.wiley.com/terms-and-conditions) on Wiley Online Library for rules of use; OA articles are governed by the applicable Creative Commons License

TABLE 3 | Considered near-fault seismic records.

#	Earthquake	Date	Mg	PGA (m/sec^2)	Site	Epic. Distance (Km)	PGA/ PGV (sec^{-1})	Specific energy density (m^2/ sec)	Soil (EC 8 class.)
46	Imperial Valley-06	Oct. 15, 1979	6.53	1.763	EC County Center FF	7.31	3.23	0.4562	C
47	Imperial Valley-06	Oct. 15, 1979	6.53	3.708	EC Meloland Overpass FF	0.07	3.23	0.9452	C
48	Imperial Valley-06	Oct. 15, 1979	6.53	3.503	El Centro-Array Sta 4	7.05	4.50	0.9552	C
49	Imperial Valley-06	Oct. 15, 1979	6.53	3.683	El Centro-Array Sta 5	3.95	4.03	1.2192	C
50	Imperial Valley-06	Oct. 15, 1979	6.53	4.333	El Centro-Array Sta 6	1.35	3.88	1.5172	C
51	Imperial Valley-06	Oct. 15, 1979	6.53	4.536	El Centro-Array Sta 7	0.56	4.17	1.0322	C
52	Imperial Valley-06	Oct. 15, 1979	6.53	4.591	El Centro-Array Sta 8	3.86	9.43	0.4322	C
53	Imperial Valley-06	Oct. 15, 1979	6.53	4.093	El Centro-Differential array	5.09	6.85	0.4752	C
54	Morgan Hill	Apr. 24, 1984	6.19	7.985	Coyote Lake Dam (SW Abut)	0.53	12.82	0.1872	B
55	Loma Prieta	Oct. 17, 1989	6.93	2.885	Gilroy. Gavilan Coll.	9.96	9.35	0.0372	B
56	Loma Prieta	Oct. 17, 1989	6.93	9.260	LGPC	3.88	9.52	1.8122	B
57	Landers	June. 28, 1992	7.28	6.911	Lucerne	2.19	5.05	2.1892	B
58	Landers	June. 28, 1992	7.28	2.313	Yermo Fire Station	23.62	4.10	0.6112	C
59	Northridge-01	Jan. 17, 1994	6.69	6.054	Jensen Filter Plant	5.43	6.21	1.0702	B
60	Northridge-01	Jan. 17, 1994	6.69	5.080	Jensen Filter Plant Generator	5.43	7.52	0.7872	B
61	Northridge-01	Jan. 17, 1994	6.69	7.098	Newhall–Fire Station	5.92	5.92	0.8712	C
62	Northridge-01	Jan. 17, 1994	6.69	4.176	Newhall–W Pico Canyon Rd.	5.48	4.76	0.8982	C
63	Northridge-01	Jan. 17, 1994	6.69	8.533	Rinaldi Receiving Station	6.5	5.10	1.2272	C
64	Northridge-01	Jan. 17, 1994	6.69	5.830	Sylmar–Converter Station	5.35	4.48	1.9942	C
65	Northridge-01	Jan. 17, 1994	6.69	8.127	Sylmar–Converter Station East	5.19	7.14	0.8242	B
66	Northridge-01	Jan. 17, 1994	6.69	7.187	Sylmar–Olive view Med FF	5.30	5.85	1.0042	B
67	Kobe, Japan	Jan. 17, 1995	6.9	8.380	KJMA	0.96	8.77	1.0032	C
68	Kobe, Japan	Jan. 17, 1995	6.9	6.330	Takarazuka	0.27	8.70	0.3712	C
69	Kocaeli, Turkey	Aug. 17, 1999	7.51	2.367	Gebze	10.92	4.63	0.4682	B
70	Chi-Chi, Taiwan	Sept. 21, 1999	7.62	6.513	CHY028	3.14	8.40	0.5592	B
71	Chi-Chi, Taiwan	Sept. 21, 1999	7.62	3.758	CHY101	9.96	5.00	1.1422	C
72	Chi-Chi, Taiwan	Sept. 21, 1999	7.62	2.808	TCU049	3.78	6.10	0.7612	B
73	Chi-Chi, Taiwan	Sept. 21, 1999	7.62	3.681	TCU052	0.66	2.22	7.2102	B
74	Chi-Chi, Taiwan	Sept. 21, 1999	7.62	2.202	TCU053	5.97	5.38	0.5292	B
75	Chi-Chi, Taiwan	Sept. 21, 1999	7.62	1.538	TCU054	5.30	2.54	0.8612	B

(Continues)

scm, 2026, 1, Downloaded from https://onlinelibrary.wiley.com/doi/10.1155/stc/8260623 by M. De Iuliis - Politecnico Di Torino Sist. Bibl Del Polit Di Torino , Wiley Online Library on [18/08/2026]. See the Terms and Conditions (https://onlinelibrary.wiley.com/terms-and-conditions) on Wiley Online Library for rules of use; OA articles are governed by the applicable Creative Commons License

TABLE 3 | (Continued)

#	Earthquake	Date	Mg	PGA (m/sec^2)	Site	Epic. Distance (Km)	PGA/ PGV (sec^{-1})	Specific energy density (m^2/ sec)	Soil (EC 8 class.)
76	Chi-Chi, Taiwan	Sept. 21, 1999	7.62	5.538	TCU068	0.32	3.00	13.8932	B
77	Chi-Chi, Taiwan	Sept. 21, 1999	7.62	3.245	TCU075	0.91	3.66	1.8322	B
78	Chi-Chi, Taiwan	Sept. 21, 1999	7.62	3.045	TCU076	2.76	4.48	0.6212	B
79	Chi-Chi, Taiwan	Sept. 21, 1999	7.62	2.302	TCU082	5.18	3.98	0.9992	B
80	Chi-Chi, Taiwan	Sept. 21, 1999	7.62	1.248	TCU087	7.00	2.86	0.6852	B
81	Chi-Chi, Taiwan	Sept. 21, 1999	7.62	2.083	TCU101	2.13	3.05	0.9102	C
82	Chi-Chi, Taiwan	Sept. 21, 1999	7.62	2.899	TCU102	1.51	2.66	1.9732	B
83	Chi-Chi, Taiwan	Sept. 21, 1999	7.62	1.305	TCU103	6.10	2.10	1.2302	B
84	Chi-Chi, Taiwan	Sept. 21, 1999	7.62	2.195	TCU122	9.35	5.18	0.7462	B
85	Chi-Chi, Taiwan	Sept. 21, 1999	7.62	2.969	WGK	9.96	4.39	0.9892	C

scm, 2026, 1, Downloaded from https://onlinelibrary.wiley.com/doi/10.1155/stc/8260623 by M. De Iuliis - Politecnico Di Torino Sist. Bibl Del Polit Di Torino , Wiley Online Library on [18/08/2026]. See the Terms and Conditions (https://onlinelibrary.wiley.com/terms-and-conditions) on Wiley Online Library for rules of use; OA articles are governed by the applicable Creative Commons License

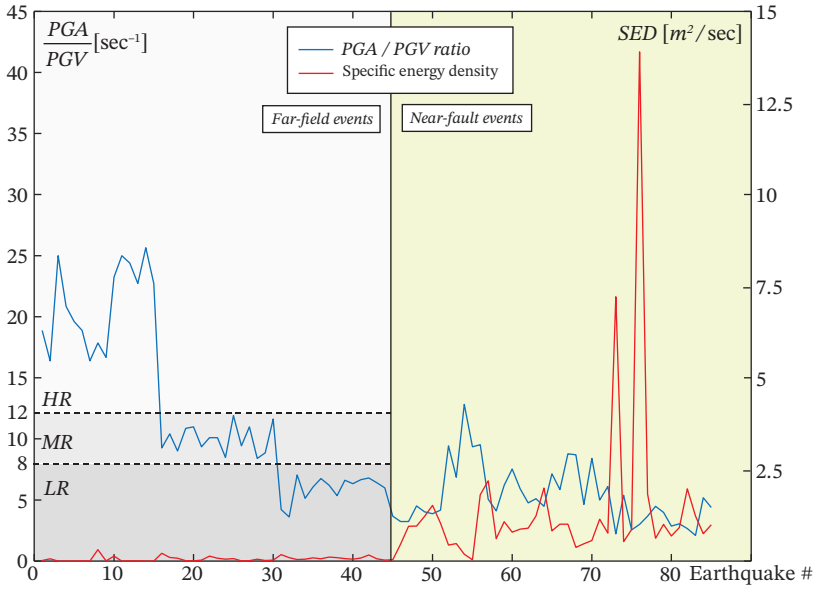

FIGURE 3 | Classification of the unscaled 85 seismic events.

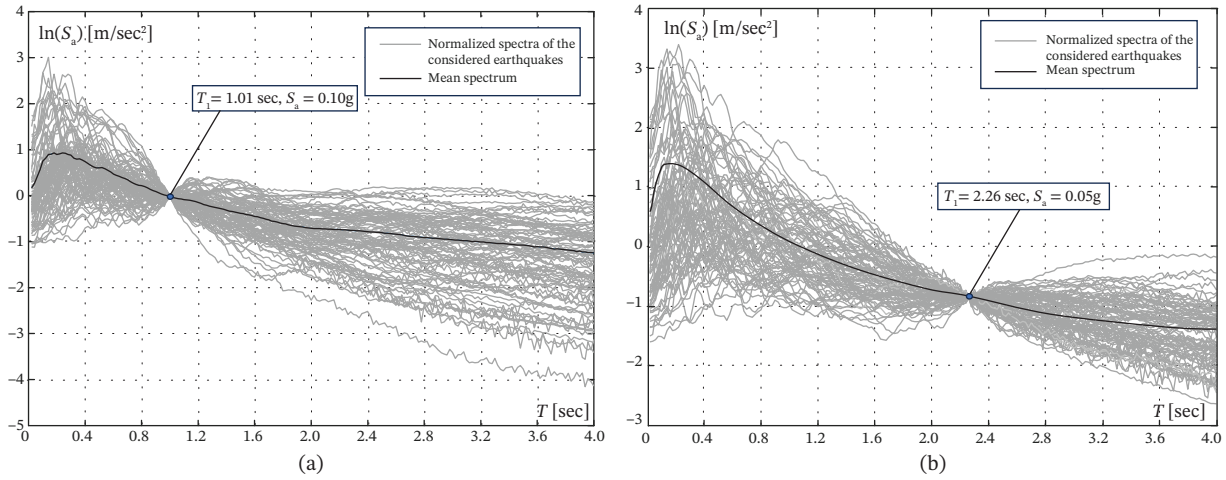

FIGURE 4 | Scaled pseudoacceleration response spectra for the considered seismic excitations: (a) BS1 and (b) BS2.

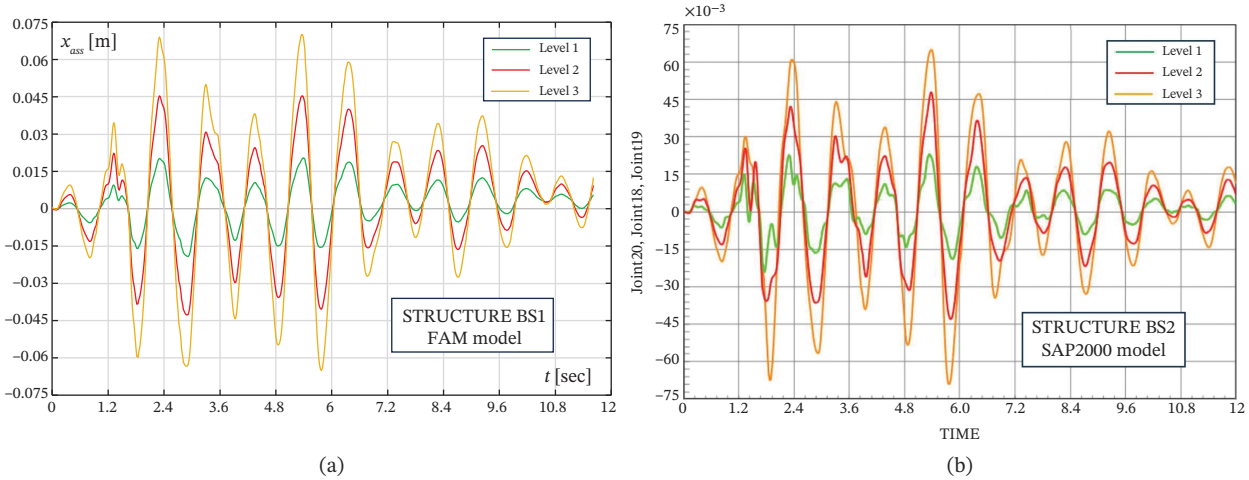

FIGURE 5 | Absolute floor displacement of structure BS1—earthquake #14. (a) FAM model and (b) SAP2000 model.

scihm, 2026, 1, Downloaded from https://onlinelibrary.wiley.com/doi/10.1155/stc/8260623 by M. De Iuliis - Politecnico Di Torino Sist. Bibl Del Polit Di Torino , Wiley Online Library on [13/08/2026]. See the Terms and Conditions (https://onlinelibrary.wiley.com/terms-and-conditions) on Wiley Online Library for rules of use; OA articles are governed by the applicable Creative Commons License

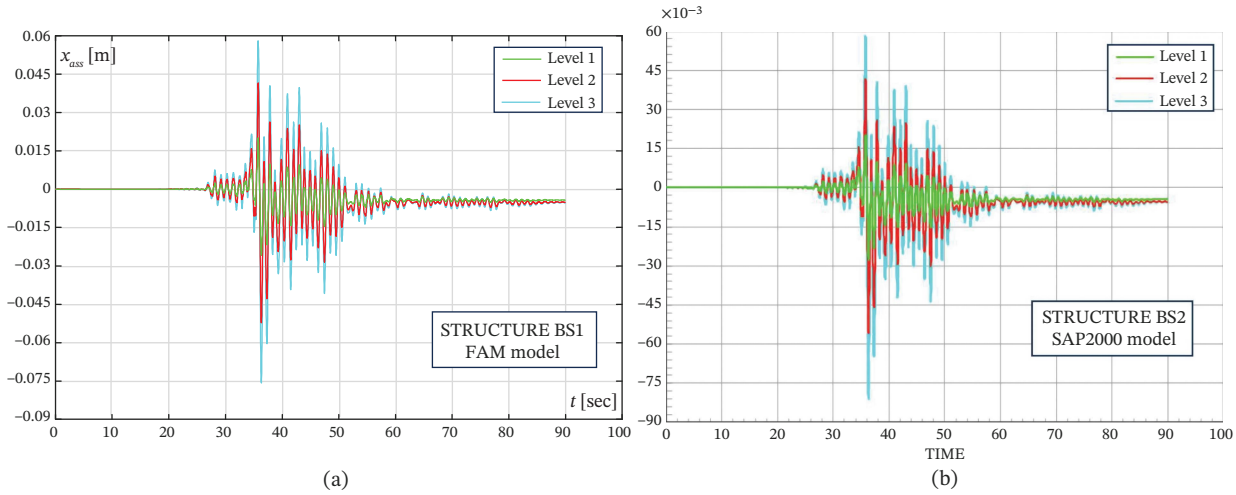

FIGURE 6 | Absolute floor displacement of structure BS1—earthquake #76. (a) FAM model and (b) SAP2000 model.

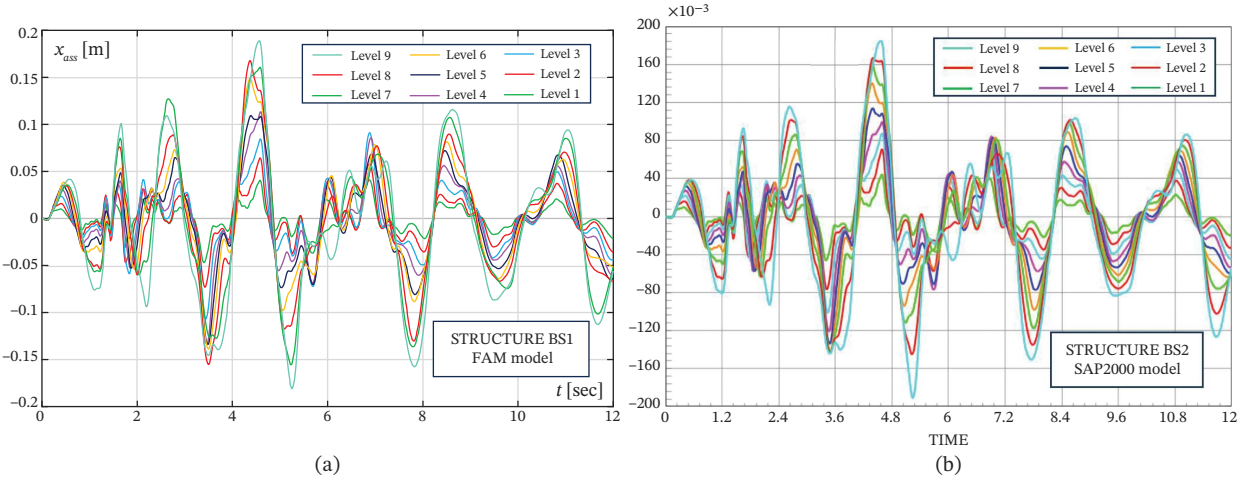

FIGURE 7 | Absolute floor displacement of structure BS2—earthquake #14. (a) FAM model and (b) SAP2000 model.

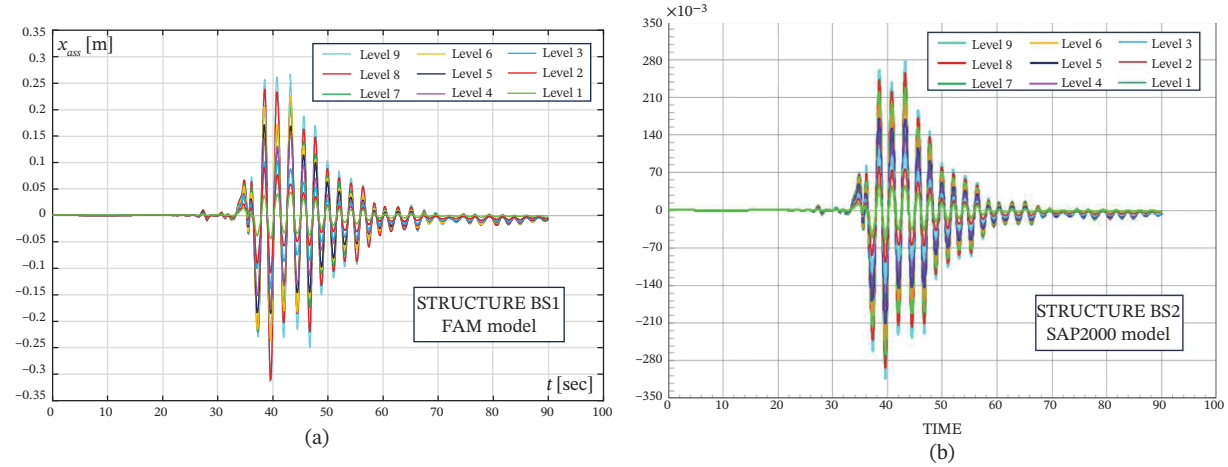

FIGURE 8 | Absolute floor displacement of structure BS2—earthquake #76. (a) FAM model and (b) SAP2000 model.

scihm, 2026, 1, Downloaded from https://onlinelibrary.wiley.com/doi/10.1155/stc/8260623 by M. De Iuliis - Politecnico Di Torino Sist. Bibl Del Polit Di Torino , Wiley Online Library on [13/08/2026]. See the Terms and Conditions (https://onlinelibrary.wiley.com/terms-and-conditions) on Wiley Online Library for rules of use; OA articles are governed by the applicable Creative Commons License

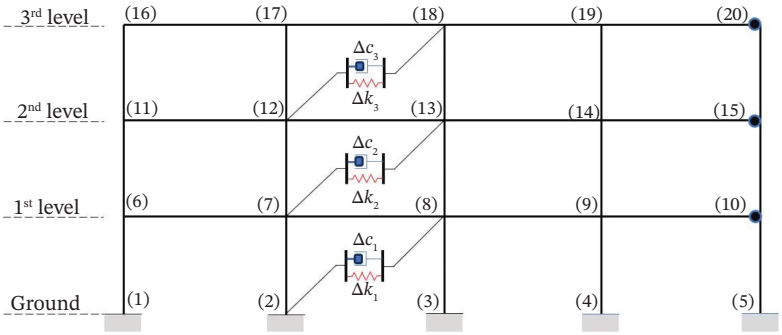

FIGURE 9 | Semiactive device layout in BS1.

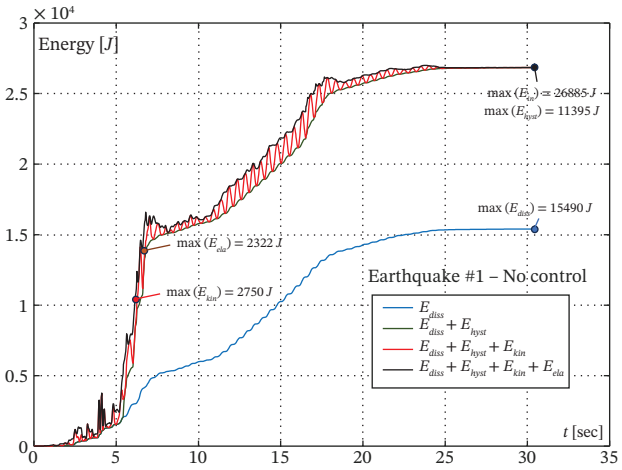

FIGURE 10 | Energy components over time: No control strategy: structure BS1.

of the energy-based semiactive control algorithms presented in this study.

5 | Effectiveness of the Proposed Semiactive Control Algorithms

With the aim of verifying the effectiveness of the proposed semiactive control algorithms summarized in Table 1, the nonlinear seismic response of two benchmark framed structures, BS1 and BS2, both assumed to have Rayleigh proportional damping corresponding to 5% in the first mode, was investigated under the described set of seismic excitations having markedly different dynamic characteristics.

Semiactive devices capable of adjusting both their damping and stiffness properties between zero and specific maximum values were considered for both structures and were arranged to operate on interstory velocities and displacements, i.e., they were connected between two consecutive floors along the full height of the building (Figure 9). This configuration is the one most commonly adopted in practical applications and was therefore selected as the reference layout for the present study. It should be noted, however, that the formulation of the algorithms provides a general criterion for controlling the different energy components: any configuration of the devices can be directly defined through the appropriate specification of the force generation and localization matrices (i.e., B_C, F_C, B_K, and F_K). In this regard, the definition of these matrices is inherently general and naturally extends to three-dimensional and irregular structural configurations, where they are assembled based on the topology and connectivity of the devices, accounting for all translational and rotational degrees of freedom without requiring any modification of the underlying formulation.

For the two reference cases, the matrices assume the following formulations:

$$B_{C,BS1} = \begin{bmatrix} 1 & 0 & 0 \\ -1 & 1 & 0 \\ 0 & -1 & 1 \end{bmatrix}, \quad F_{C,BS1} = I_3 = \begin{bmatrix} 1 & 0 & 0 \\ 0 & 1 & 0 \\ 0 & 0 & 1 \end{bmatrix}, \tag{33}$$

$$B_{C,BS2} = \begin{bmatrix} 1 & 0 & 0 & 0 & 0 & 0 & 0 & 0 & 0 \\ -1 & 1 & 0 & 0 & 0 & 0 & 0 & 0 & 0 \\ 0 & -1 & 1 & 0 & 0 & 0 & 0 & 0 & 0 \\ 0 & 0 & -1 & 1 & 0 & 0 & 0 & 0 & 0 \\ 0 & 0 & 0 & -1 & 1 & 0 & 0 & 0 & 0 \\ 0 & 0 & 0 & 0 & -1 & 1 & 0 & 0 & 0 \\ 0 & 0 & 0 & 0 & 0 & -1 & 1 & 0 & 0 \\ 0 & 0 & 0 & 0 & 0 & 0 & -1 & 1 & 0 \\ 0 & 0 & 0 & 0 & 0 & 0 & 0 & -1 & 1 \end{bmatrix}, \quad F_{C,BS2} = I_9. \tag{34}$$

The maximum values for both damping and stiffness properties were set to be compatible with engineering applications. Specifically, the maximum damping was designed to provide an extrastructural equivalent damping ratio equal to 10% of the critical damping in the first mode for both structural systems, and the maximum stiffness was selected to produce an increase in the first-mode frequency of $1.20\,Hz$ for BS1 and $0.75\,Hz$ for BS2, assuming all semiactive devices are activated.

In terms of equivalent structural control parameters, the adopted bounds correspond to a maximum damping coefficient increment of $\Delta C_{\max} = 500\,kN \cdot s/m$ per story for BS1 and $\Delta C_{\max} = 250\,kN \cdot s/m$ per story for BS2. The associated stiffness increment is defined at structural level as $\Delta K_{\max} = 14000\,kN/m$ and $\Delta K_{\max} = 15000\,kN/m$ per story, respectively. These values are consistent with experimentally validated ranges reported in the literature for large-scale MR damping systems and semiactive stiffness-modulated bracing systems, where damping devices provide significant velocity-dependent dissipation while stiffness modulation is achieved through auxiliary structural elements such as lockup or switchable braces [64, 65]. This formulation ensures physically meaningful constraints and enables a consistent comparison of the proposed control strategies under realistic implementation limits.

schm, 2026, 1, Downloaded from https://onlinelibrary.wiley.com/doi/10.1155/stc/8260623 by M. De Iuliis - Politecnico Di Torino Sist. Bibl Del Polit Di Torino , Wiley Online Library on [13/08/2026]. See the Terms and Conditions (https://onlinelibrary.wiley.com/terms-and-conditions) on Wiley Online Library for rules of use; OA articles are governed by the applicable Creative Commons License

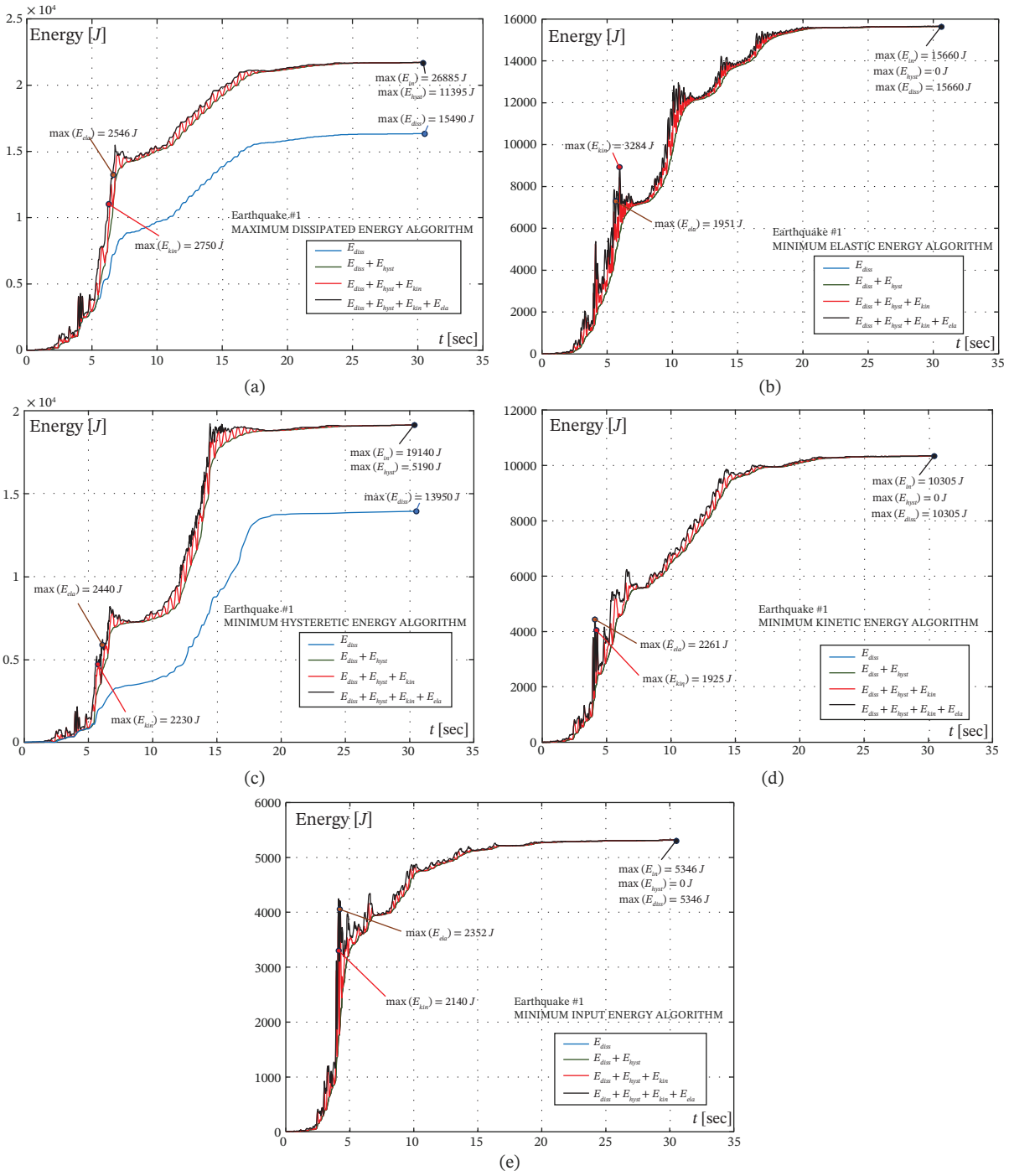

FIGURE 11 | Energy components over time: Semiactive control strategy: structure BS1.

While the above formulation treats the semiactive devices as elements with directly adjustable damping and stiffness properties, real devices such as MR dampers exhibit nonlinear force–velocity behavior that goes beyond this idealization [15, 16]. The direct integration of the proposed algorithms with real devices would, therefore, require the adoption of appropriate device characterization procedures to extract equivalent linear properties [23].

For comparative purposes, in addition to the five control strategies proposed in this work, the seismic response of the benchmark structures was studied under three other control strategies.

1. No control: all damping and stiffness resources are inactive;
2. Passive control: all damping and stiffness resources are active;
3. KK and/or SH semiactive algorithms: additional stiffness resources are activated based on the Kamagata and Kobori (KK) algorithm [18, 19], whereas extrastructural damping resources follow the Sky–Hook (SH) algorithm [66–68].

Regarding the KK algorithm, it follows the intuitive idea that maximum stiffness is activated when the relative displacement and velocity at the level "l" where the device is installed have the

scihm, 2026, 1, Downloaded from https://onlinelibrary.wiley.com/doi/10.1155/stc/8260623 by M. De Iuliis - Politecnico Di Torino Sist. Bibl Del Polit Di Torino , Wiley Online Library on [13/08/2026]. See the Terms and Conditions (https://onlinelibrary.wiley.com/terms-and-conditions) on Wiley Online Library for rules of use; OA articles are governed by the applicable Creative Commons License

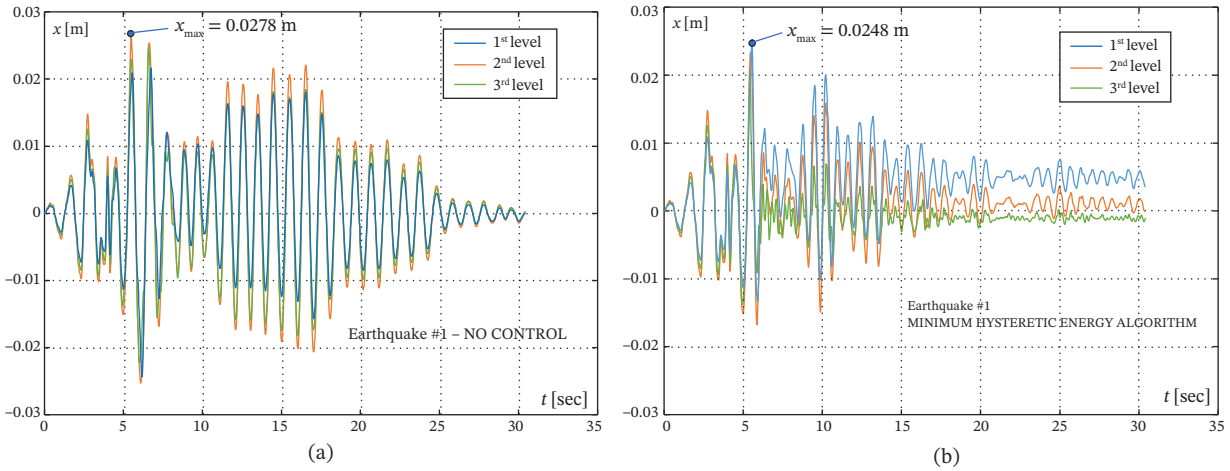

FIGURE 12 | Comparison between no control and minimum hysteretic energy algorithm: structure BS1.

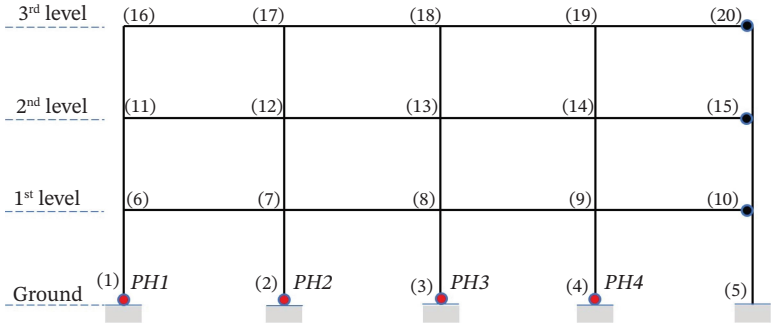

FIGURE 13 | Plastic hinge configuration for earthquake #1: uncontrolled structure BS1.

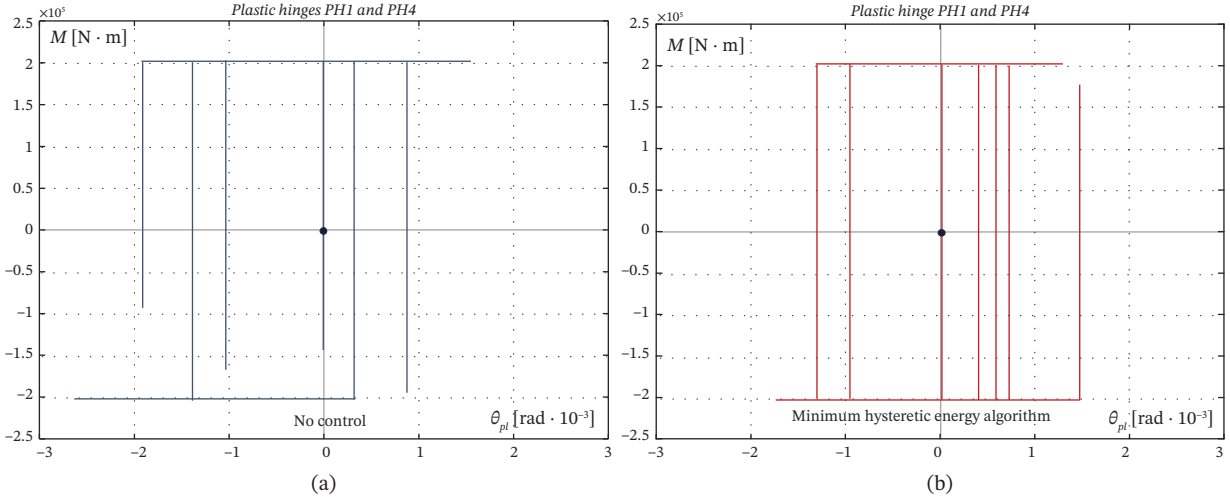

FIGURE 14 | Comparison of moment–plastic rotation diagrams: earthquake #1 and structure BS1.

same direction, mimicking the human equilibrium process, as explained in the following:

$$\begin{cases} \Delta k_l \geq 0 & \text{if } X_l \cdot \dot{X}_l \geq 0, \\ \Delta k_l < 0 & \text{if } X_l \cdot \dot{X}_l < 0. \end{cases} \tag{35}$$

whereas the SH algorithm is designed to emulate the ideal damping value known as "Sky–Hook damping", in which the linear viscous device generates a force proportional to the absolute velocity of the mass, which is particularly effective in reducing seismic energy transmission from the ground to the

schm, 2026, 1, Downloaded from https://onlinelibrary.wiley.com/doi/10.1155/stc/8260623 by M. De Iuliis - Politecnico Di Torino Sist. Bibl Del Polit Di Torino , Wiley Online Library on [13/08/2026]. See the Terms and Conditions (https://onlinelibrary.wiley.com/terms-and-conditions) on Wiley Online Library for rules of use; OA articles are governed by the applicable Creative Commons License

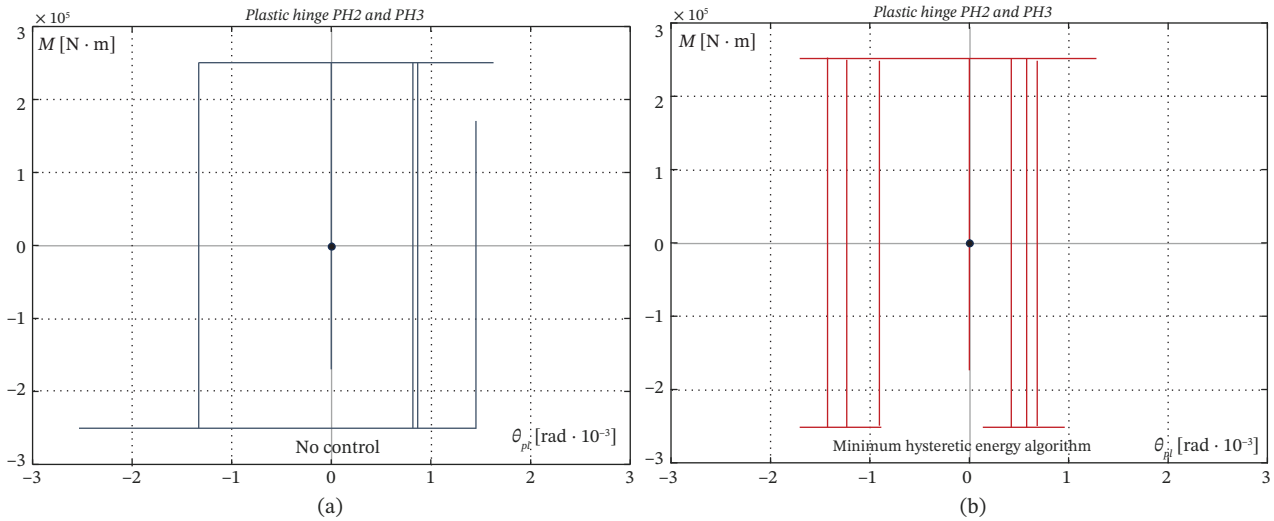

FIGURE 15 | Comparison of moment–plastic rotation diagrams: earthquake #1 and structure BS1.

structural system. This algorithm is specified by the following simple control law of equation:

$$\begin{cases} \Delta c_l \geq 0 \quad \text{if } X_l \cdot \left(\sum_{k=1}^{l} \dot{X}_k + \dot{U}_g \right) \geq 0, \\ \Delta c_l < 0 \quad \text{if } X_l \cdot \left(\sum_{k=1}^{l} \dot{X}_k + \dot{U}_g \right) < 0. \end{cases} \tag{36}$$

These two algorithms were selected for comparison from the various proposals available in the literature because they exhibit a level of complexity and a framework similar to those proposed in this work. In fact, they do not aim to track the optimal action defined by an active control law but rather to tune the semiactively controlled parameters based on the dynamic state of the device.

It is also worth noting that the observed smooth and stable behavior of the proposed control laws suggests a limited sensitivity to small time delays, as the control actions are defined through algebraic switching conditions.

Figures 10–24 present the significant results from the extensive numerical simulations carried out.

Figures 10–11 show the time histories of the different energy terms (Equation (7)) for the first earthquake of the considered set and for the structure BS1. Specifically, Figure 10 presents the case of no control, while Figures 11a-11e show the results when the semiactive devices are regulated according to the five proposed algorithms: maximization of dissipated energy (Figure 11a), minimization of elastic energy (Figure 11b), minimization of hysteretic energy (Figure 11c), minimization of kinetic energy (Figure 11d) and minimization of input energy (Figure 11e).

Figures 10–11 also highlight the maximum values for the five energy rates referred to the different algorithms. It is straightforward to verify that, in this specific case, the individual semiactive control algorithms are effective in reducing the respective energy terms compared to both the uncontrolled scenario and those in which an algorithm targeting a different energy objective is considered. When performing this comparison, it should be noted that, in the case of the elastic and hysteretic energy minimization algorithm (Figure 11b,c), the comparison should be carried out with the response of the uncontrolled structure (Figure 10), that is, by considering the same level of available damping.

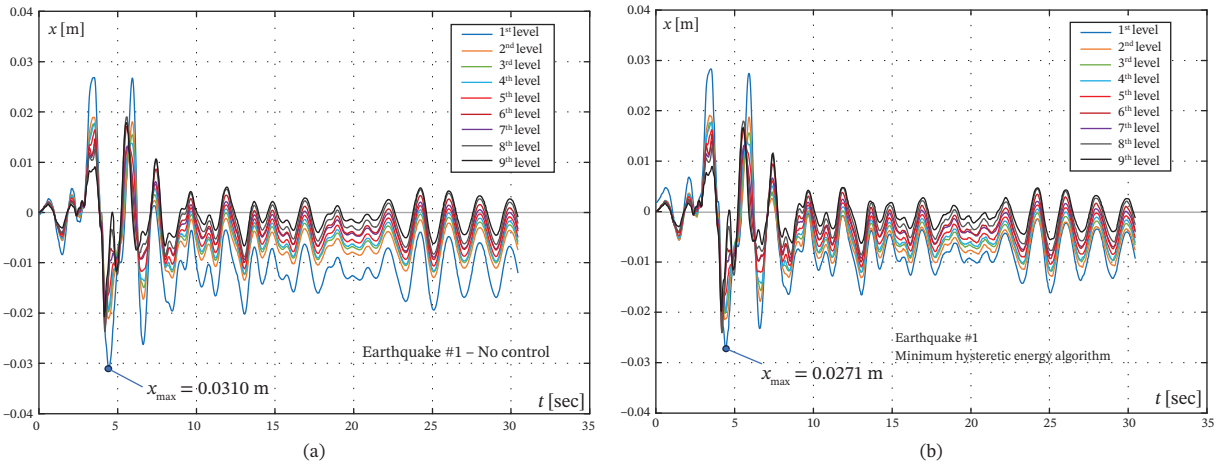

FIGURE 16 | Comparison between no control and minimum hysteretic energy algorithm: structure BS2.

scihm, 2026, 1, Downloaded from https://onlinelibrary.wiley.com/doi/10.1155/stc/8260623 by M. De Iuliis - Politecnico Di Torino Sist. Bibl Del Polit Di Torino , Wiley Online Library on [13/08/2026]. See the Terms and Conditions (https://onlinelibrary.wiley.com/terms-and-conditions) on Wiley Online Library for rules of use; OA articles are governed by the applicable Creative Commons License

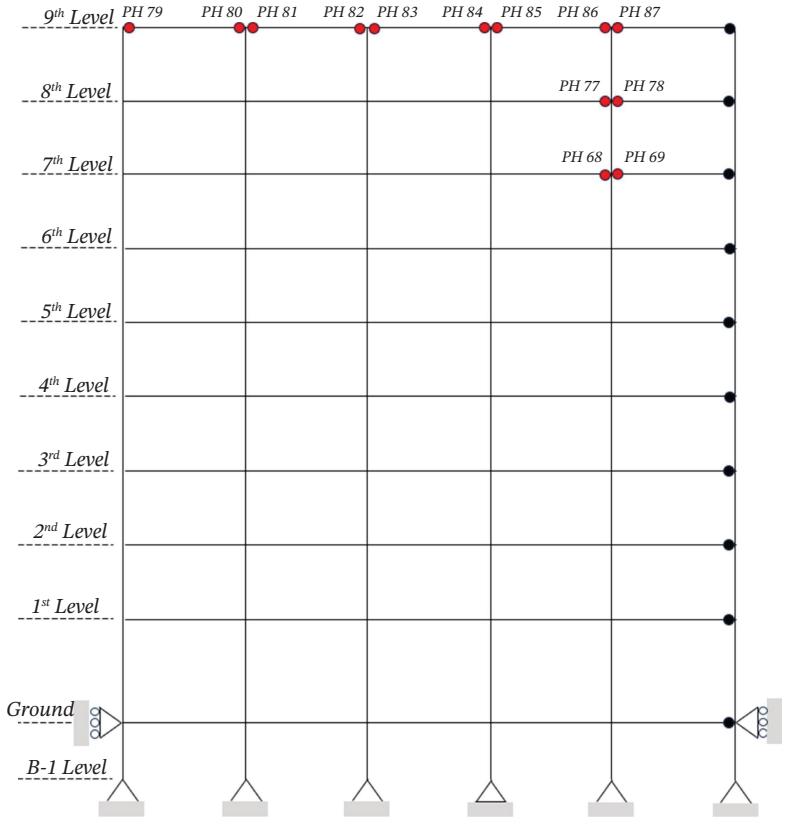

FIGURE 17 | Plastic hinge configuration for earthquake #1: uncontrolled structure BS2.

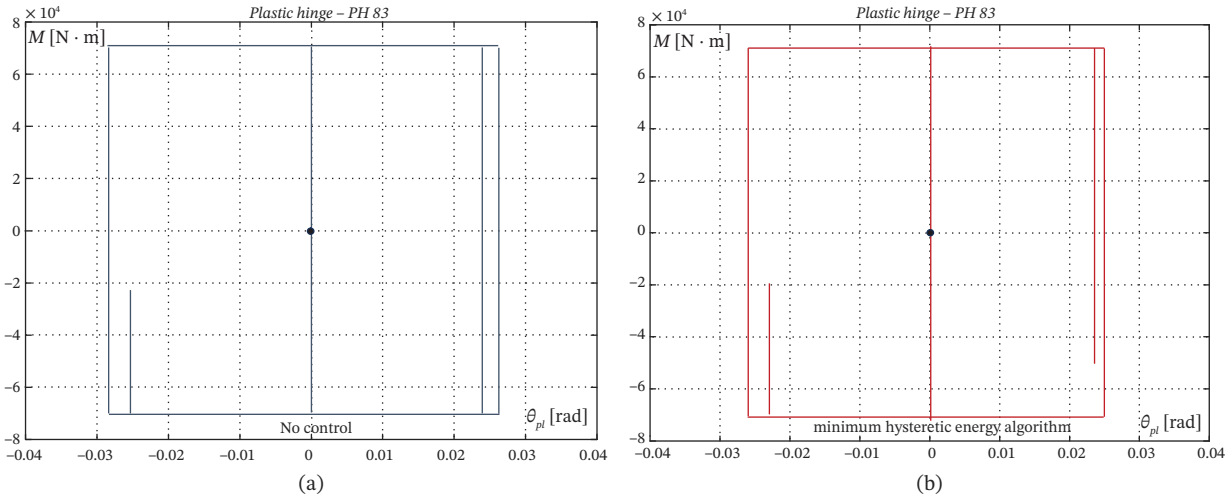

FIGURE 18 | Comparison of moment–plastic rotation diagrams: earthquake #1 and structure BS2.

For the same seismic excitation and the BS1 structure, Figure 12 shows the time history of the interstory relative displacements in the uncontrolled case (Figure 12a) and in the case of the structure controlled by an algorithm aimed at minimizing the hysteretic energy (Figure 12b). As highlighted by Equation (22), this algorithm adopts a decision rule based on a nonlinear term; therefore, it becomes effective only after the system experiences its first excursion into the plastic range. The control action is intended to limit the development of plastic hinges and their plastic excursions, with the aim of reducing the overall level of structural damage. Figure 13 illustrates the configuration of the plastic hinges in the structure under consideration, while Figures 14 and 15 present the moment–rotation diagrams in the plastic range of these plastic hinges.

Figures 16–19 present the results of the same analyses carried out for the second structural system, BS2, considered to test the proposed control algorithms.

schm, 2026, 1, Downloaded from https://onlinelibrary.wiley.com/doi/10.1155/stc/8260623 by M. De Iuliis - Politecnico Di Torino Sist. Bibl Del Polit Di Torino , Wiley Online Library on [13/08/2026]. See the Terms and Conditions (https://onlinelibrary.wiley.com/terms-and-conditions) on Wiley Online Library for rules of use; OA articles are governed by the applicable Creative Commons License

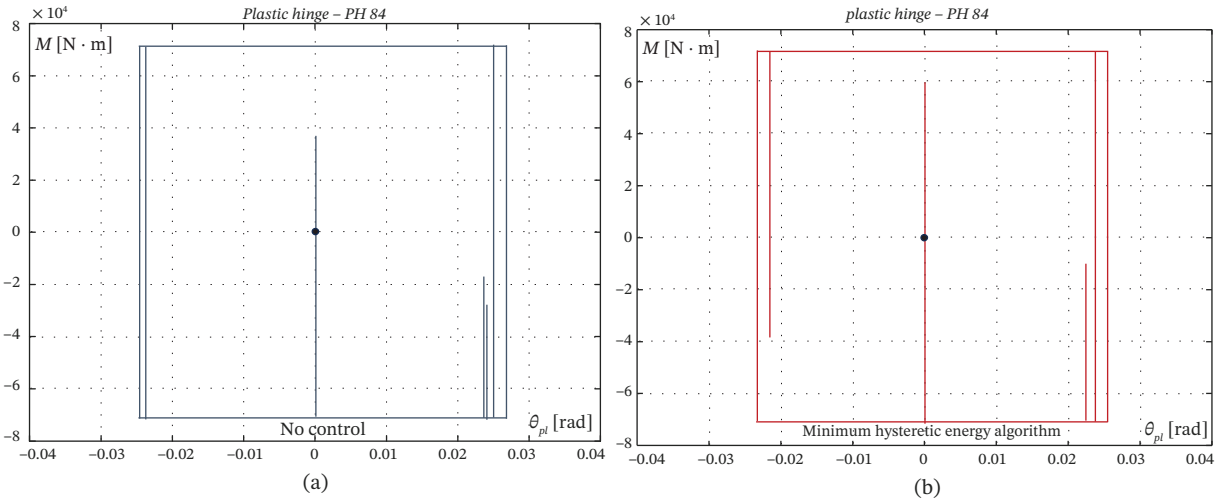

FIGURE 19 | Comparison of moment–plastic rotation diagrams: earthquake #1 and structure BS2.

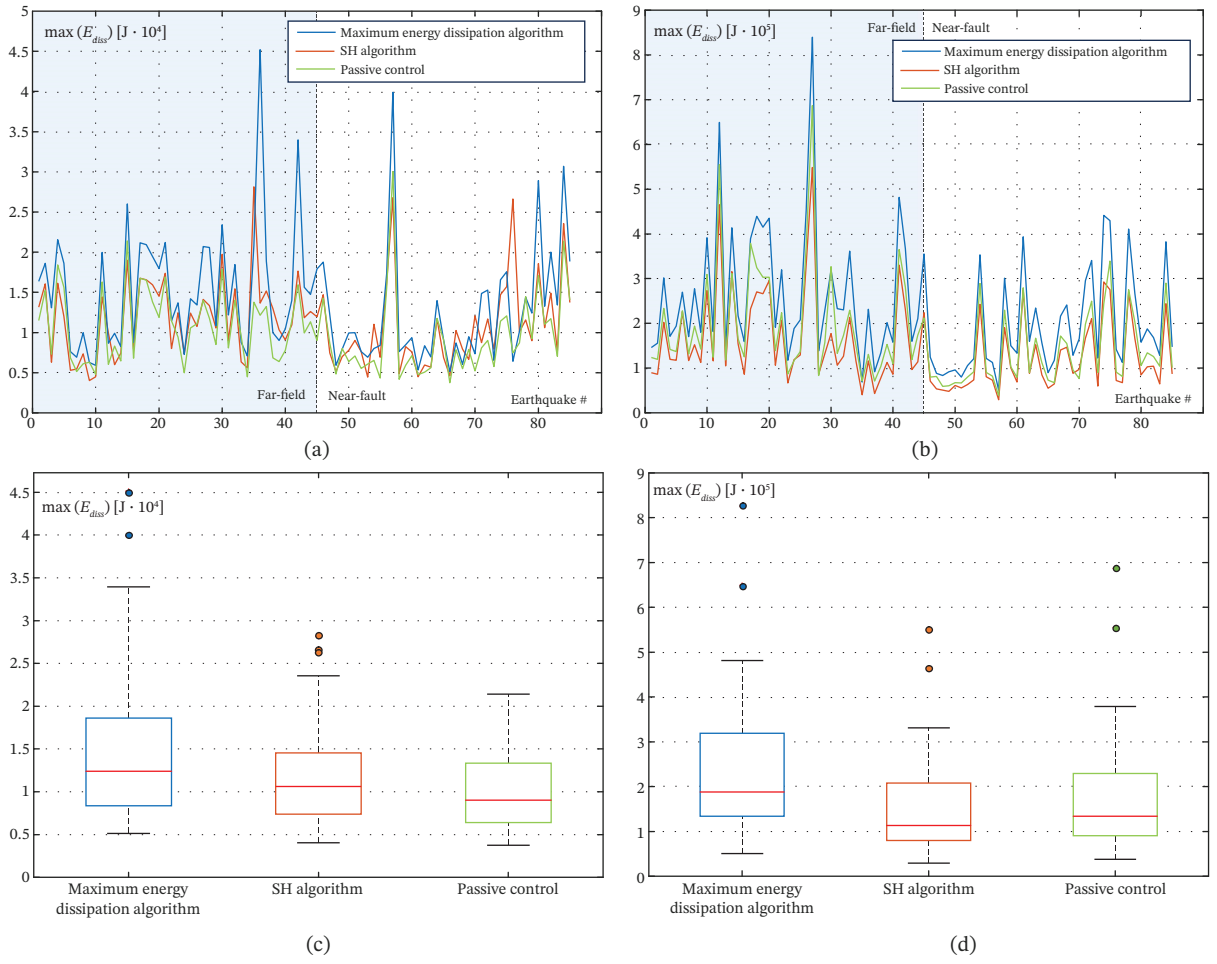

FIGURE 20 | Maximum dissipated energy: comparison between different algorithms: (a), (c) BS1 and (b), (d) BS2.

scihm, 2026, 1, Downloaded from https://onlinelibrary.wiley.com/doi/10.1155/stc/8260623 by M. De Iuliis - Politecnico Di Torino Sist. Bibl Del Polit Di Torino , Wiley Online Library on [13/08/2026]. See the Terms and Conditions (https://onlinelibrary.wiley.com/terms-and-conditions) on Wiley Online Library for rules of use; OA articles are governed by the applicable Creative Commons License

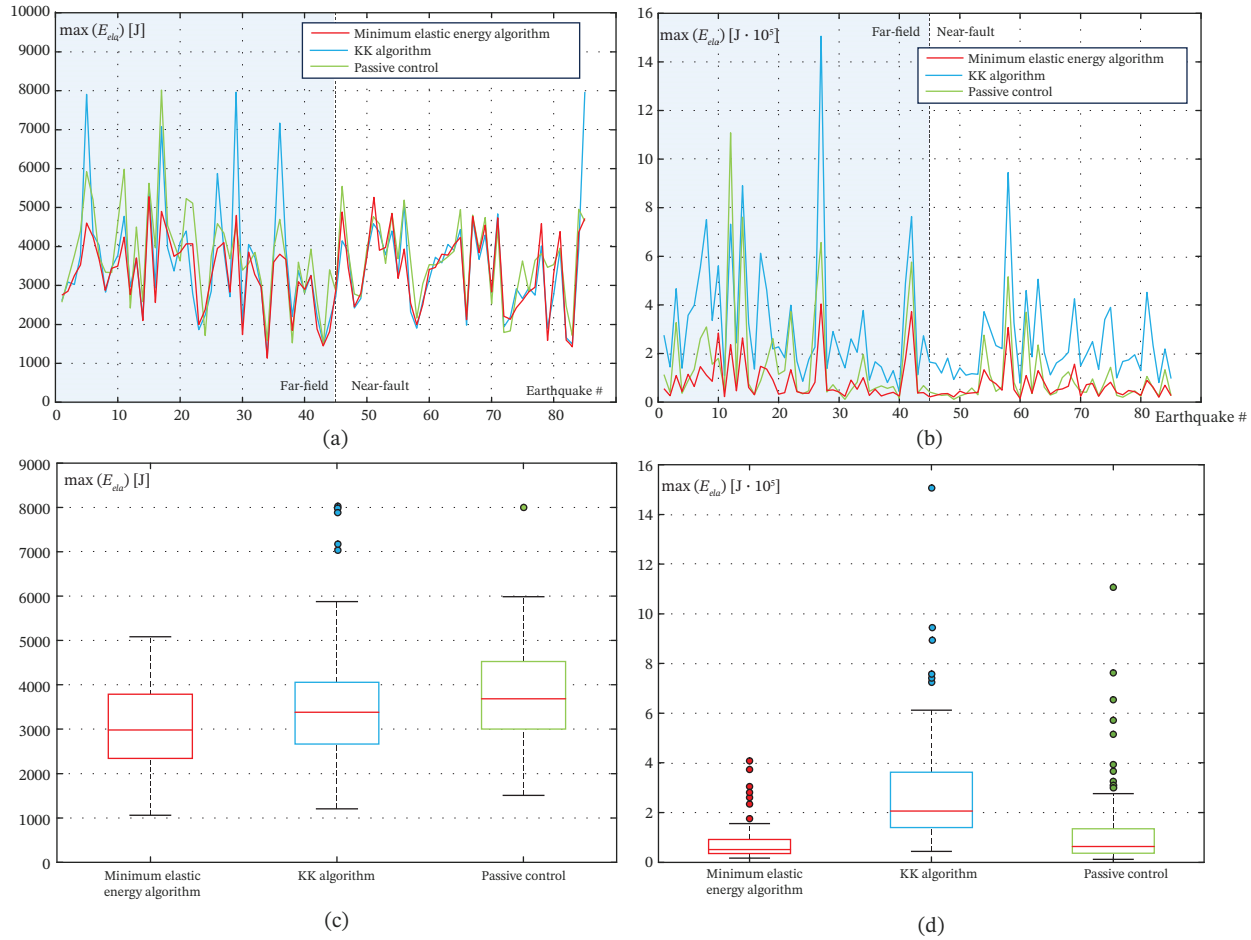

FIGURE 21 | Minimum elastic energy: comparison between different algorithms: (a), (c) BS1 and (b), (d) BS2.

The reported results highlight, for the considered seismic event, the effectiveness of the hysteretic energy minimization algorithm for both of the investigated structures. Specifically, in the BS1 structure, the four plastic hinges at the base of the columns form almost simultaneously; therefore, the effectiveness of the control action is reflected in the limitation of the maximum plastic rotation and in the reduction of the number of hysteretic cycles characterizing each individual plastic hinge, rather than through a significant redistribution of plastic demand. Conversely, for the BS2 structure, the plastic hinges indicated in Figure 17 refer to the nonlinear response of the uncontrolled system. In this second case, the algorithm leads to the formation of a smaller number of plastic hinges (PH77, PH78, and PH68 do not develop in the controlled system), as well as to a reduced development of hysteretic cycles in the remaining hinges, indicating a more pronounced influence of control on the global damage pattern. This difference highlights how structural flexibility plays a role in determining the dominant mechanism through which the control strategy affects nonlinear response.

With the aim of investigating the effectiveness of the proposed algorithms for all the considered seismic excitations, Figures 20–24 present, for both structures, the maximum energy rates associated with the semiactive algorithms for each seismic input. In particular, for each proposed algorithm, plots (a) and (b) compare, for the BS1 and BS2 structures, respectively, this energy measure with that obtained using the KK and/or SH algorithms, depending on whether the proposed algorithm addresses the control of stiffness only, damping only, or both dynamic properties, as well as with the passive strategy involving the constant-in-time application of the available supplemental damping and stiffness resources. In the same figures, to enhance the readability of the results, plots (c) and (d) show box plots of the distribution of the maximum values obtained for each seismic event, with reference to the three different control strategies considered.

The analysis results indicate that the proposed strategies achieve significant improvements over the KK and SH reference algorithms and exhibit good robustness to variations in seismic characteristics. In terms of energy management, algorithms aimed at maximizing dissipated energy and minimizing the various energy components exhibit distinct yet complementary behaviors. Maximization of dissipated energy (i.e., Figure 20) leads to average increases of approximately 15%–20% compared to the SH strategy, with particularly evident benefits for high-energy NF events, along with a reduction in response dispersion, indicating greater overall reliability. At the same time, elastic energy minimization (i.e., Figure 21) proves to be highly effective in limiting the deformation energy accumulated in the structure, approaching the performance of passive control while avoiding the continuous activation of maximum stiffness; in this case, average reductions of up to 25%–30% are observed relative to the

scihm, 2026, 1, Downloaded from https://onlinelibrary.wiley.com/doi/10.1155/stc/8260623 by M. De Iuliis - Politecnico Di Torino Sist. Bibl Del Polit Di Torino , Wiley Online Library on [13/08/2026]. See the Terms and Conditions (https://onlinelibrary.wiley.com/terms-and-conditions) on Wiley Online Library for rules of use; OA articles are governed by the applicable Creative Commons License

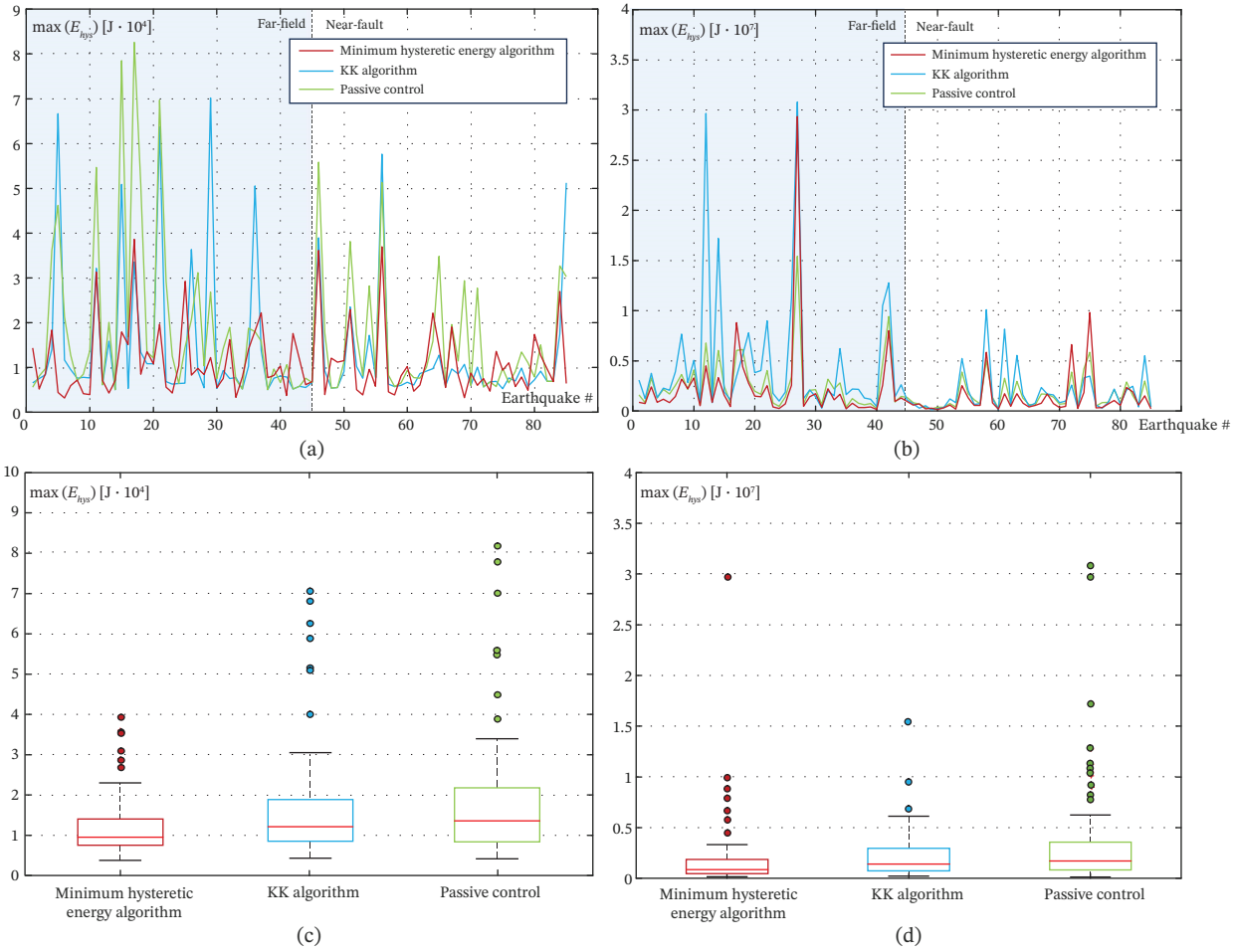

FIGURE 22 | Minimum hysteretic energy: comparison between different algorithms: (a), (c) BS1 and (b), (d) BS2.

KK algorithm, especially for events characterized by medium-to-high PGA/PGV ratios.

Among the strategies analyzed, hysteretic energy minimization (i.e., Figure 22) emerges as the most significant contribution in terms of protecting the structural system against severe damage limit states. The results indicate significant reductions in energy dissipated through hysteresis, on the order of 30%–45% compared to the KK control, with even more pronounced benefits for NF events, which typically induce more severe nonlinear excursions. These reductions translate directly into lower plastic rotations, fewer plastic hinges, and an overall lower level of damage, confirming the effectiveness of the approach even under the most severe seismic scenarios.

The input energy minimization algorithm (i.e., Figure 23), on the other hand, significantly reduces the energy transferred from the ground motion to the structure, with average reductions of up to 30%–35% for the BS1 structure and more moderate results for BS2, likely due to the greater flexibility of the system. This strategy is particularly effective for FF events with high PGA/PGV ratios; however, it tends to promote greater dynamic coupling with the base motion, making it not always optimal for all structural configurations. By contrast, kinetic energy minimization proves particularly effective in limiting the absolute velocities of the structure, with average reductions of up to 35%–40%, especially in the presence of impulsive NF events, thereby contributing to reduced acceleration demands and enhanced protection of nonstructural components.

A global comparison of the five strategies highlights that hysteretic energy minimization and elastic energy minimization offer the greatest benefits in terms of structural performance and damage control, while strategies based on energy dissipation and input/kinetic energy represent intermediate solutions capable of balancing different performance objectives. It is also important to note that all the proposed algorithms exhibit a generally lower dispersion of responses than the reference control methods, confirming greater robustness with respect to seismic input variability. Finally, the intrinsic computational efficiency of the FAM approach makes these algorithms fully implementable in real time, without the need for iterative procedures or continuous updates of stiffness matrices, which is a crucial aspect for practical applications in structural control systems.

In addition to the energy-based performance indices discussed above, Figures 25 and 26 present the box plot distributions of two classical structural control performance indices: the peak interstory displacement (Figure 25a,b) and the peak absolute floor acceleration (Figure 26a,b), evaluated over the full set of 85 seismic records, for both benchmark structures and all considered control strategies, including the no-control reference case. These two indices were selected as the most representative and complementary indicators for assessing the effectiveness of the

scihm, 2026, 1, Downloaded from https://onlinelibrary.wiley.com/doi/10.1155/stc/8260623 by M. De Iuliis - Politecnico Di Torino Sist. Bibl Del Polit Di Torino , Wiley Online Library on [13/08/2026]. See the Terms and Conditions (https://onlinelibrary.wiley.com/terms-and-conditions) on Wiley Online Library for rules of use; OA articles are governed by the applicable Creative Commons License

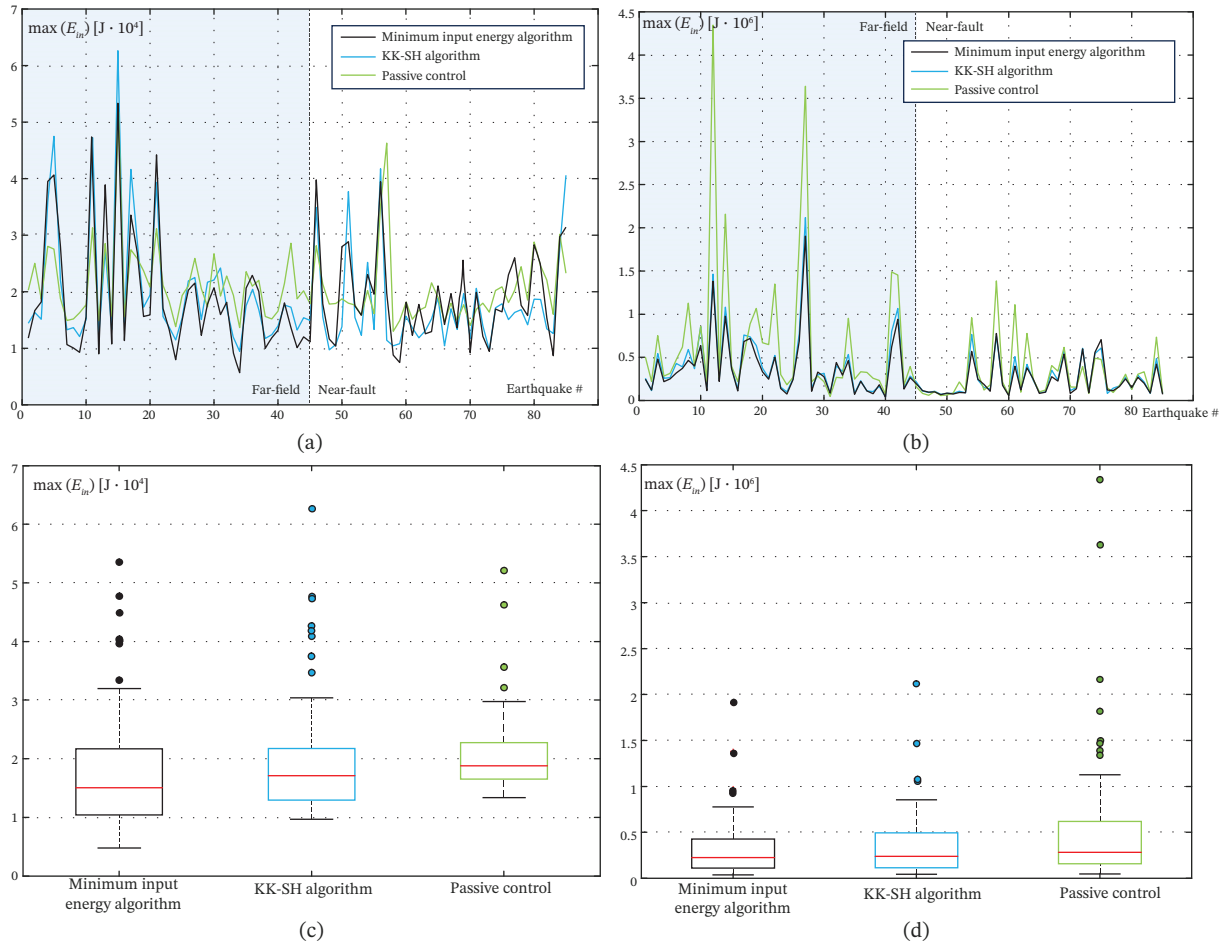

FIGURE 23 | Minimum input energy: comparison between different algorithms: (a), (c) BS1 and (b), (d) BS2.

proposed algorithms from a conventional structural engineering perspective. Peak interstory displacement is directly related to the level of structural damage, as it governs the extent of plastic excursions in the load-bearing members and the associated residual deformations. Peak absolute floor acceleration, on the other hand, is the primary parameter controlling the response of nonstructural components and building contents and is, therefore, of particular relevance for performance-based seismic design. Together, these two indices capture the two main dimensions of seismic performance (structural safety and serviceability) and are the most widely adopted benchmarks in the structural control literature, enabling a direct comparison with existing works.

The results confirm that the proposed algorithms achieve consistent improvements also in terms of these conventional structural performance indices. Regarding peak interstory displacement, the hysteretic energy minimization, and elastic energy minimization strategies prove to be the most effective in both structures, yielding the largest reductions in median response and dispersion, consistent with their explicit objective of limiting plastic excursions and stored deformation energy. The kinetic energy minimization and input energy minimization algorithms show more moderate improvements in terms of displacement, as their control objectives are not directly oriented toward limiting structural deformation.

Regarding peak absolute floor acceleration, a physically relevant result emerges: the elastic energy minimization algorithm, while highly effective in reducing displacements, produces acceleration demands comparable to or higher than the no-control case in both structures. This behavior is attributable to the additional stiffness introduced by the control action, which shifts the structural frequencies and amplifies the contribution of higher vibration modes to the acceleration response, an effect that is more pronounced in BS1 and partially present in BS2. By contrast, the kinetic energy minimization algorithm consistently achieves the lowest acceleration demands among all strategies, confirming its direct effectiveness on velocity- and acceleration-related response quantities. These results highlight a trade-off between displacement and acceleration performance that should be carefully considered in practical applications, depending on whether the primary design objective is structural damage limitation or protection of nonstructural components and building contents.

The overall picture emerging from the numerical investigation carries direct implications for engineering practice. None of the five strategies, considered individually, offers a general optimal solution but rather addresses distinct and partially competing performance objectives, and their selection should, therefore, be guided by the dominant design criterion. Structural damage limitation under inelastic excursions naturally calls for hysteretic energy minimization, while the protection of acceleration-

scihm, 2026, 1, Downloaded from https://onlinelibrary.wiley.com/doi/10.1155/stc/8260623 by M. De Iuliis - Politecnico Di Torino Sist. Bibl Del Polit Di Torino , Wiley Online Library on [13/08/2026]. See the Terms and Conditions (https://onlinelibrary.wiley.com/terms-and-conditions) on Wiley Online Library for rules of use; OA articles are governed by the applicable Creative Commons License

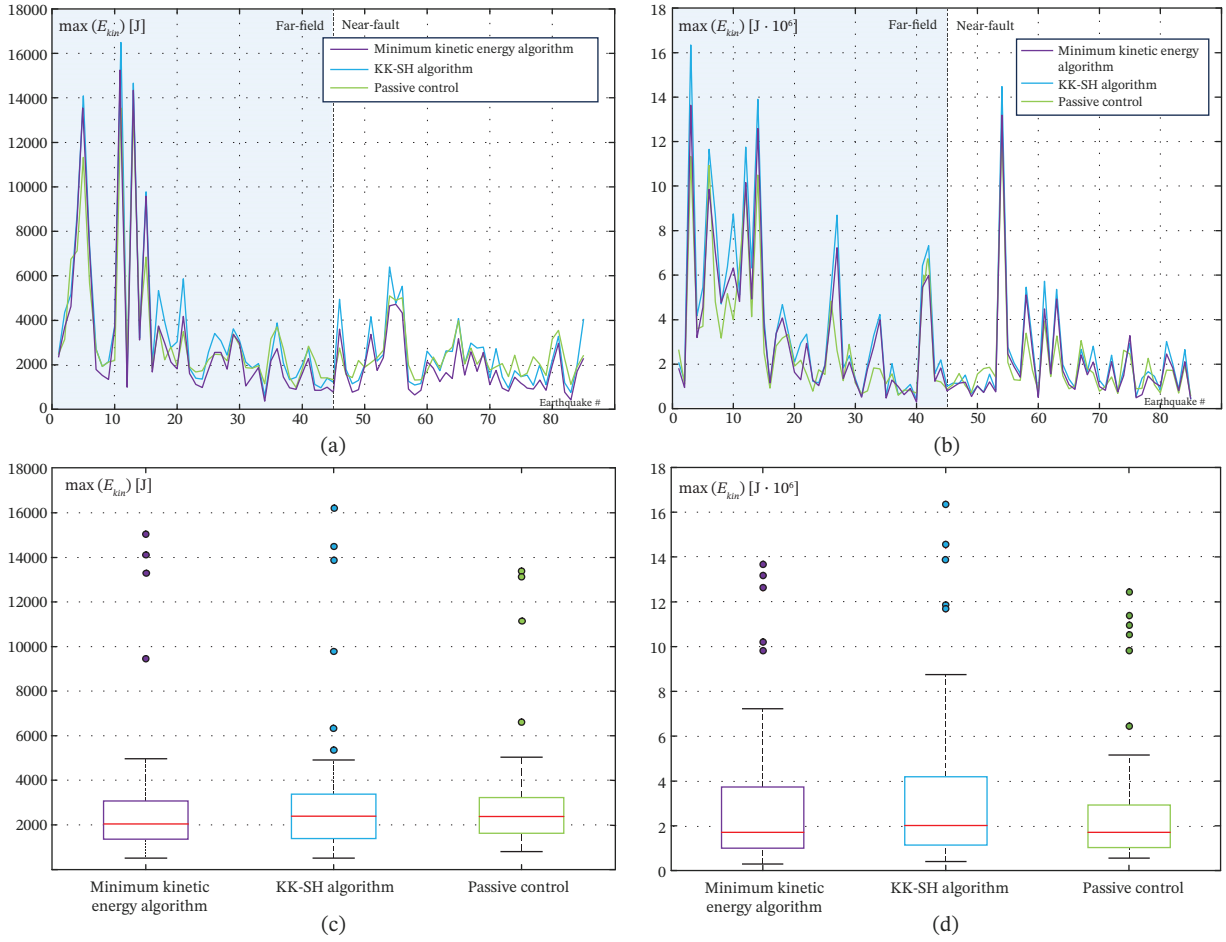

FIGURE 24 | Minimum kinetic energy: comparison between different algorithms: (a), (c) BS1 and (b), (d) BS2.

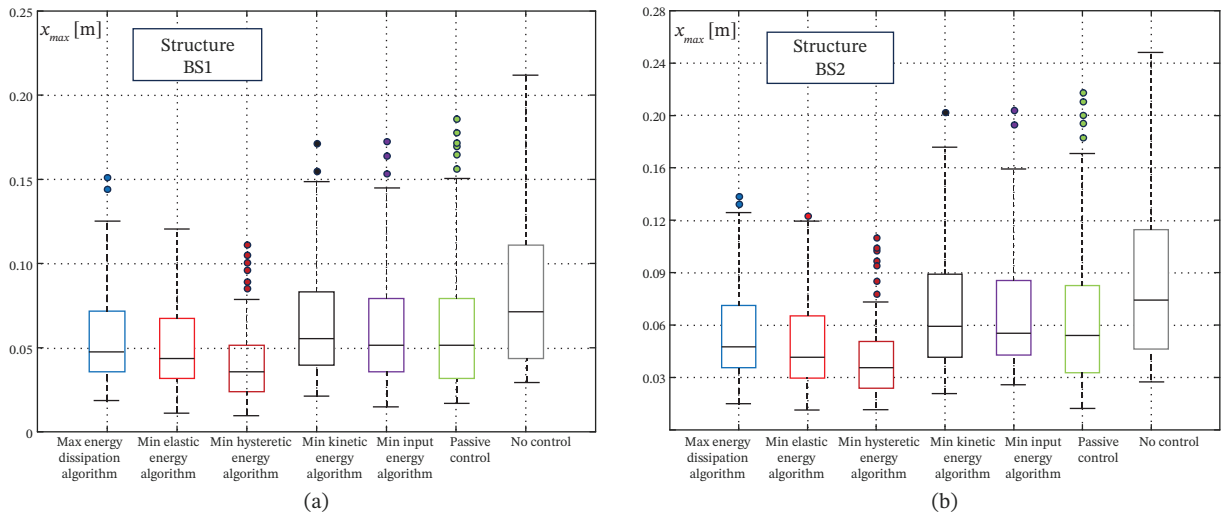

FIGURE 25 | Peak interstory displacement: comparison between different algorithms. (a) BS1 and (b) BS2.

scihm, 2026, 1, Downloaded from https://onlinelibrary.wiley.com/doi/10.1155/stc/8260623 by M. De Iuliis - Politecnico Di Torino Sist. Bibl Del Polit Di Torino , Wiley Online Library on [13/08/2026]. See the Terms and Conditions (https://onlinelibrary.wiley.com/terms-and-conditions) on Wiley Online Library for rules of use; OA articles are governed by the applicable Creative Commons License

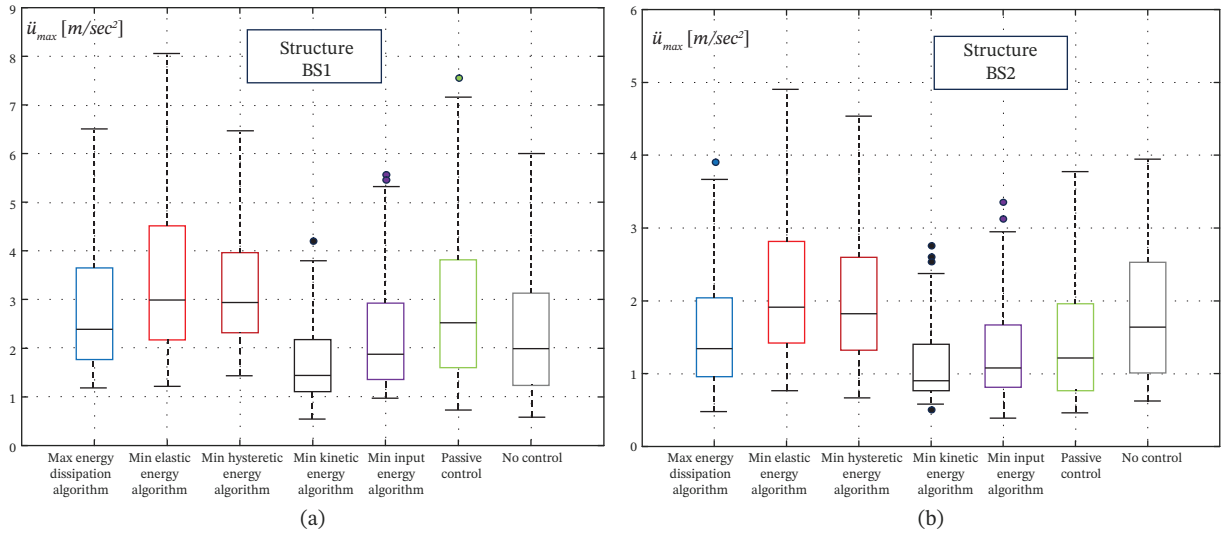

FIGURE 26 | Peak absolute floor acceleration: comparison between different algorithms. (a) BS1 and (b) BS2.

sensitive nonstructural components finds its most direct expression in kinetic energy minimization. When the design is framed within an energy-based perspective aimed at controlling the total seismic demand transferred to the structural system, input energy minimization represents the most coherent criterion, whereas elastic energy minimization is the preferred choice whenever deformation control and elastic range preservation are paramount. The maximization of dissipated energy, finally, constitutes a robust general-purpose strategy when no single performance objective dominates and the goal is to exploit the full force capacity of the semiactive devices.

6 | Conclusion

The present study has proposed a unified and physically grounded framework for the development of semiactive control algorithms for framed structures exhibiting nonlinear seismic response. The approach is formulated within the context of the FAM, which enables the derivation of closed-form, real-time control laws through the minimization or maximization of selected energy rate components governing the structural dynamic behavior. Within this framework, five energy-based semiactive control strategies have been developed, targeting dissipated, elastic, hysteretic, kinetic, and input energy, and expressed through explicit algebraic relations that regulate the stiffness and damping properties of semiactive devices based on directly measurable response quantities, including displacements, velocities, and plastic rotations at potential hinge locations.

The performance of the proposed algorithms has been assessed through numerical simulations on two benchmark steel MRFs, representing low- and midrise structures, subjected to a set of 85 natural ground motions encompassing both FF and NF conditions. The results indicate that all strategies achieve, on average, their respective energy control objectives and provide improvements over established semiactive control approaches of comparable complexity, such as the KK and SH algorithms. Depending on the control objective, structural configuration, and seismic input characteristics, reductions in the targeted energy components generally range between 15% and more than 50%, demonstrating the effectiveness of the proposed formulation.

Hysteretic energy minimization is particularly effective in limiting structural damage, producing reductions in hysteretic energy dissipation, plastic rotations, and plastic hinge formation, especially under NF excitations. More generally, the proposed algorithms show stable performance across the full set of seismic records, with reduced dispersion of response measures relative to benchmark strategies, indicating robustness with respect to variations in seismic demand.

By selecting different energy rate components as control objectives, the proposed methodology provides a systematic and physically transparent criterion for identifying the most appropriate strategy depending on the specific seismic performance target, whether structural damage limitation, acceleration control, or overall energy management. In addition, the FAM-based formulation ensures computational efficiency and real-time applicability, as all control actions are obtained through explicit expressions without iterative procedures or continuous stiffness matrix updates. The consistency of these findings is further confirmed by the results in terms of classical structural performance indices: the hysteretic energy minimization strategy proves to be the most effective in limiting peak interstory displacements, while the kinetic energy minimization algorithm achieves the largest reductions in peak absolute floor accelerations, highlighting a displacement–acceleration trade-off that should be accounted for in practical applications depending on the primary design objective.

Although time delays associated with sensing, processing, or actuation are not explicitly considered, their influence is expected to primarily affect the timing of switching events defined by the control laws rather than the overall structural response. A detailed assessment of delay effects can be investigated in future work.

Furthermore, the present study focuses on planar frame systems with interstory semiactive devices and idealized hinge models; these aspects provide a clear and interpretable basis for evaluation. While the proposed framework is formulated in terms of equivalent linear device properties and is, therefore, compatible with a broad class of semiactive technologies, its direct application to real hardware requires device-specific characterization

scihm, 2026, 1, Downloaded from https://onlinelibrary.wiley.com/doi/10.1155/stc/8260623 by M. De Iuliis - Politecnico Di Torino Sist. Bibl Del Polit Di Torino , Wiley Online Library on [13/08/2026]. See the Terms and Conditions (https://onlinelibrary.wiley.com/terms-and-conditions) on Wiley Online Library for rules of use; OA articles are governed by the applicable Creative Commons License

procedures to extract equivalent mechanical properties from the nonlinear force–velocity response. The experimental validation of the proposed algorithms with real devices and the assessment of the associated implementation uncertainties are identified as priorities for future research, together with the extension of the framework to more complex hysteretic models, alternative device configurations, three-dimensional systems, and additional sources of uncertainty, including soil–structure interaction and life-cycle performance assessment, as well as the development of a multiobjective optimization framework, based on Pareto front analysis, for the systematic selection among competing control strategies.

Funding

No funding was received for this manuscript.

Open access publishing was facilitated by Politecnico di Torino, as part of the Wiley-CRUI-CARE agreement.

Disclosure

This work is part of the collaborative activity developed by the authors within the research project "RELUIS-WP15 Dispositivi e sistemi di Isolamento e Dissipazione."

Conflicts of Interest

The authors declare no conflicts of interest.

Data Availability Statement

The data that support the findings of this study are available from the corresponding author upon reasonable request.

References

1. T. T. Soong, *Active Structural Control: Theory and Practice* (Longman Scientific & Technical, 1990).

2. T. T. Soong and G. F. Dargush, *Passive Energy Dissipation Systems in Structural Engineering* (John Wiley & Sons, 1997).

3. J. M. Kelly, *Earthquake-Resistant Design With Rubber* (Springer, 1997).

4. A. K. Chopra, *Dynamics of Structures: Theory and Applications to Earthquake Engineering*, 4th ed. (Prentice Hall, 2012).

5. B. F. Spencer and M. K. Sain, "Controlling Buildings: A New Frontier in Feedback," *IEEE Control Systems Magazine* 17, no. 6 (1997): 19–35, https://doi.org/10.1109/37.642972.

6. T. T. Soong, "Introduction to Active Control," in *CISM International Centre for Mechanical Sciences*, ed. T. T. Soong and M. C. Costantinou, 345 (Vienna: Passive and Active Structural Vibration Control in Civil Engineering. CISM International Centre for Mechanical Sciences, 1994), 271–274, https://doi.org/10.1007/978-3-7091-3012-4_13.

7. S. J. Dyke, B. F. Spencer, P. Quast, D. C. Kaspari, and M. K. Sain, "Implementation of an Active Mass Driver Using Acceleration Feedback Control," *Computer-Aided Civil and Infrastructure Engineering* 11, no. 5 (1996): 305–323, https://doi.org/10.1111/j.1467-8667.1996.tb00445.x.

8. M. P. Singh, E. E. Matheu, and L. E. Suarez, "Active and Semi-Active Control of Structures Under Seismic Excitation," *Earthquake Engineering and Structural Dynamics* 26, no. 2 (1997): 193–213, https://doi.org/10.1002/(SICI)1096-9845(199702)26:2%3c193::AID-EQE634%3e3.0.CO;2-%23.

9. M. D. Symans and M. C. Constantinou, "Semi-Active Control Systems for Seismic Protection of Structures: A State-of-the-Art Review," *Engineering Structures* 21, no. 6 (1999): 469–487, https://doi.org/10.1016/S0141-0296(97)00225-3.

10. Z.-D. Xu, Y.-L. Zhao, Y.-Q. Guo, X.-L. Yang, and W. Sarwar, "Shaking Table Tests of Magnetorheological Damped Frame to Mitigate the Response Under Real-Time Online Control," *Smart Materials and Structures* 28, no. 11 (2019): 115021, https://doi.org/10.1088/1361-665X/ab45fd.

11. M. D. Christie, S. Sun, L. Deng, et al., "The Variable Resonance Magnetorheological Pendulum Tuned Mass Damper: Mathematical Modelling and Seismic Experimental Studies," *Journal of Intelligent Material Systems and Structures* 31, no. 2 (2020): 263–276, https://doi.org/10.1177/1045389X19888799.

12. M. D. Christie, S. Sun, L. Deng, et al., "A Variable Resonance Magnetorheological-Fluid-Based Pendulum Tuned Mass Damper for Seismic Vibration Suppression," *Mechanical Systems and Signal Processing* 116 (2019): 530–544, https://doi.org/10.1016/j.ymssp.2018.07.007.

13. D. Cruze, H. Gladston, E. N. Farsangi, S. Loganathan, T. Dharmaraj, and S. M. Solomon, "Development of a Multiple Coil Magneto-Rheological Smart Damper to Improve the Seismic Resilience of Building Structures," *Open Civil Engineering Journal* 14, no. 1 (2020): 78–93, https://doi.org/10.2174/1874149502014010078.

14. A. Ghaffary and R. Karami Mohammadi, "Comprehensive Nonlinear Seismic Performance Assessment of MR Damper Controlled Systems Using Virtual Real-Time Hybrid Simulation," *Structural Design of Tall and Special Buildings* 28, no. 8 (2019): e1606, https://doi.org/10.1002/tal.1606.

15. Jr., B. F. Spencer, S. J. Dyke, M. K. Sain, and J. D. Carlson, "Phenomenological Model of a Magnetorheological Damper," *Journal of Engineering Mechanics* 123, no. 3 (1997): 230–238, https://doi.org/10.1061/(ASCE)0733-9399(1997)123:3(230).

16. S. J. Dyke, Jr., B. F. Spencer, M. K. Sain, and J. D. Carlson, "Modeling and Control of Magnetorheological Dampers for Seismic Response Reduction," *Smart Materials and Structures* 5, no. 5 (1996): 565–575, https://doi.org/10.1088/0964-1726/5/5/006.

17. A. Nishitani, Y. Nitta, and Y. Ikeda, "Semiactive Structural Control Based on Variable Slip-Force Level Dampers," *Journal of Structural Engineering* 129, no. 7 (2003): 933–940, https://doi.org/10.1061/(ASCE)0733-9445(2003)129:7(933).

18. T. Kobori, "Active Variable Stiffness System-Active Seismic Response Control," *Proc. US-Italy-Japan Workshop/Symposium on Structural Control and Intelligent Systems* 1992 (1992): 140–153.

19. S. Kamagata, "Autonomous Adaptive Control of Active Variable Stiffness System for Seismic Ground Motion," *Proceedings of the First World Conference on Structural Control* 2 (1994): TA4–33.

20. S. Nagarajaiah and S. Sahasrabudhe, "Seismic Response Control of Smart Sliding Isolated Buildings Using Variable Stiffness Systems: Experimental and Numerical Study," *Earthquake Engineering and Structural Dynamics* 35, no. 2 (2006): 177–197, https://doi.org/10.1002/eqe.514.

21. D. T. R. Pasala, A. A. Sarlis, S. Nagarajaiah, A. M. Reinhorn, M. C. Constantinou, and D. Taylor, "Adaptive Negative Stiffness: New Structural Modification Approach for Seismic Protection," *Journal of Structural Engineering* 139, no. 7 (2013): 1112–1123, https://doi.org/10.1061/(ASCE)ST.1943-541X.0000615.

22. J. R. Høgsberg and S. Krenk, "Adaptive Tuning of Elasto-Plastic Damper," *International Journal of Non-Linear Mechanics* 42, no. 7 (2007): 928–940, https://doi.org/10.1016/j.ijnonlinmec.2007.04.003.

23. T. K. Caughey, "Equivalent Linearization Techniques," *Journal of the Acoustical Society of America* 35, no. 11 (1965): 1706–1711, https://doi.org/10.1121/1.1918794.

24. J. B. Roberts and P. D. Spanos, *Random Vibration and Statistical Linearization* (Dover Publications, 2003).

scihm, 2026, 1, Downloaded from https://onlinelibrary.wiley.com/doi/10.1155/stc/8266623 by M. De Iuliis - Politecnico Di Torino Sist. Bibl Del Polit Di Torino , Wiley Online Library on [13/08/2026]. See the Terms and Conditions (https://onlinelibrary.wiley.com/terms-and-conditions) on Wiley Online Library for rules of use; OA articles are governed by the applicable Creative Commons License

25. L. S. Pontryagin, V. G. Boltyanskii, R. V. Gamkrelidze, and E. F. Mishchenko, *The Mathematical Theory of Optimal Processes* (Interscience, 1962).

26. H. K. Khalil, *Nonlinear Systems*, 3rd ed. (Prentice Hall, 2002).

27. M. Bitaraf, O. E. Ozbulut, S. Hurlebaus, and L. Barroso, "Application of Semi-Active Control Strategies for Seismic Protection of Buildings With MR Dampers," *Engineering Structrures* 32, no. 10 (2010): 3040–3047, https://doi.org/10.1016/j.engstruct.2010.05.023.

28. D. Karnopp, "Active and Semi-Active Vibration Isolation," *Journal of Mechanical Design* 117 (1995): 177–185, https://doi.org/10.1115/1.2836452.

29. Q. G. Zhi and S. O. Olutunde, "Application of MR Damper in Structural Control Using ANFIS Method," *Computers & Structures* 86, no. 3–5 (2008): 427–436, https://doi.org/10.1016/j.compstruc.2007.02.024.

30. Z. Xiao, J. Xu, L. Wang, and L. Huang, "Research on Intelligent Semi-Active Control Algorithms and Seismic Reliability Based on Machine Learning," *Scientific Reports* 14, no. 1 (2024): 29487, https://doi.org/10.1038/s41598-024-74457-7.

31. J. C. Simo and T. J. R. Hughes, *Computational Inelasticity Interdisciplinary Applied Mathematics* (Springer, 1998), https://doi.org/10.1007/b98904.

32. T. H. Lin, *Theory of Inelastic Structures* (Wiley, 1968).

33. K. K. F. Wong and R. Yang, "Inelastic Dynamic Response of Structures Using Force Analogy Method," *Journal of Engineering Mechanics* 125, no. 10 (1999): 1190–1199, https://doi.org/10.1061/(ASCE)0733-9399(1999)125:10(1190).

34. V. Calofir, G. B. Nica, G. Stamatescu, and N. Arghira, "Dynamic Nonlinear Modelling of Building Structure Using the Force Analogy Method," in *2019 10th IEEE International Conference on Intelligent Data Acquisition and Advanced Computing Systems: Technology and Applications (IDAACS)* (Metz, France, September, 2019), 1068–1073, https://doi.org/10.1109/IDAACS.2019.8924408.

35. C. M. Patlán, H. Hernández-Barrios, I. F. Huergo, and F. Domínguez-Mota, "Time Integration Scheme for Nonlinear Structural Dynamics, FAM, Including Structural Vibration Control," *Computers & Structures* 308 (2025): 107645, https://doi.org/10.1016/j.compstruc.2025.107645.

36. K. K. F. Wong, "A New Analytical Method for Solving Nonlinear Stability Problems of Framed Structures," in *Proceedings of the Annual Stability Conference* (Toronto, Canada: Structural Stability Research Council, March 2014).

37. G. Li, Q. Liu, and H. Li, "Inelastic Structural Control Based on MBC and FAM," *Mathematical Problems in Engineering* 2011, no. 1 (2011): 460731, https://doi.org/10.1155/2011/460731.

38. R. I. Munteanu, G. B. Nica, V. Calofir, S. S. Iliescu, and O. T. Sîrbu, "Building Seismic Behavior Improvement Using an Optimal Control Algorithm," *IEEE International Conference on Automation, Quality and Testing* (Robotics (AQTR), Cluj-Napoca, Romania, 2020, 2020), 1–6, https://doi.org/10.1109/AQTR49680.2020.9130005.

39. M. De Iuliis, E. Miceli, and P. Castaldo, "An Energy Framework to Control Viscoelastic Semi-Active Devices in Plan-Wise One-Way Asymmetric Systems," *Structural Control and Health Monitoring* 2025, no. 1 (2025): 7091316, https://doi.org/10.1155/stc/7091316.

40. M. De Iuliis and P. Castaldo, "An Energy-Based Approach to the Seismic Control of One-Way Asymmetrical Structural Systems Using Semi-Active Devices," *Ingegneria Sismica* 29, no. 4 (2012): 31–50.

41. L. Lu, G. Lin, and C. Lin, "Absolute-Energy-Based Active Control Strategies for Linear Seismic Isolation Systems," *Structural Control and Health Monitoring* 18, no. 3 (2011): 321–340, https://doi.org/10.1002/stc.373.

42. D. H. Zelleke and V. Matsagar, "Energy-Based Predictive Algorithm for Semi-Active Tuned Mass Dampers," *Structural Design of Tall and Special Buildings* 28, no. 28 (2019): e1626, https://doi.org/10.1002/tal.1626.

43. L. Xia, D. Wu, L. Chen, and J. Li, "An Instantaneous Minimum Input Energy Control Strategy for Isolation Systems With Co-Varying Stiffness and Damping," *Institute of Electrical and Electronics Engineers Access* 13 (2025): 138235–138246, https://doi.org/10.1109/ACCESS.2025.3592026.

44. K. K. Wong, "Seismic Energy Dissipation of Inelastic Structures With Tuned Mass Dampers," *Journal of Engineering Mechanics* 142, no. Issue 2 (2008): 163–172, https://doi.org/10.1061/(ASCE)0733-9399(2008)134:2(163).

45. Ö. Şahin, N. G. Adar, M. Kemerli, et al., "A Comparative Evaluation of Semi-Active Control Algorithms for Real-Time Seismic Protection of Buildings via Magnetorheological Fluid Dampers," *Journal of Building Engineering* 42 (2021): 102795, https://doi.org/10.1016/j.jobe.2021.102795.

46. Y. Ohtori, R. E. Christenson, B. F. Spencer, and S. J. Dyke, "Benchmark Control Problems for Seismically Excited Nonlinear Buildings," *Journal of Engineering Mechanics* 130, no. Issue 4 (2004): 366–385, https://doi.org/10.1061/(ASCE)0733-9399(2004)130:4(366).

47. C. M. Uang and V. V. Bertero, "Evaluation of Seismic Energy in Structures," *Earthquake Engineering and Structural Dynamics* 19, no. 1 (1990): 77–90, https://doi.org/10.1002/eqe.4290190108.

48. F. Çalım, A. Güllü, and E. Yüksel, "A Comprehensive State-of-the-Art Review on Energy-Based Procedures in Earthquake-Resistant Structural Design," *Archives of Civil and Mechanics Engineering* 26, no. 2 (2026): 45, https://doi.org/10.1007/s43452-025-01405-1.

49. K. K. F. Wong and R. Yang, "Earthquake Response and Energy Evaluation of Inelastic Structures," *Journal of Engineering Mechanics* 128, no. 3 (2002): 308–317, https://doi.org/10.1061/(ASCE)0733-9399(2002)128:3(308).

50. S. Mahin, J. Malley, and R. Hamburger, "Overview of the FEMA/SAC Program for Reduction of Earthquake Hazards in Steel Moment Frame Structures," *Journal of Constructional Steel Research* 58, no. 5–8 (2002): 511–528, https://doi.org/10.1016/S0143-974X(01)00088-8.

51. P. Castaldo and E. Miceli, "Optimal Single Concave Sliding Device Properties for Isolated Multi-Span Continuous Deck Bridges Depending on the Ground Motion Characteristics," *Soil Dynamics and Earthquake Engineering* 173 (2023): 108128, https://doi.org/10.1016/j.soildyn.2023.108128.

52. G. P. Mavroeidis and A. S. Papageorgiou, "A Mathematical Representation of Near-Fault Ground Motions," *Bulletin of the Seismological Society of America* 93, no. 3 (2003): 1099–1131, https://doi.org/10.1785/0120020100.

53. P. G. Sommerville, "Engineering Characterization of Near Fault Ground Motions," in *Proceedings of the 2005 NZSEE Conference. Christchurch: New Zealand Society for Earthquake Engineering* (Taupo, New Zealand, February, 2005).

54. T. J. Zhu, W. K. Tso, and A. C. Heidebrecht, "Effect of Peak Ground a/v Ratio on Structural Damage," *Journal of Structural Engineering* 114, no. 5 (1988): 1019–1037, https://doi.org/10.1061/(ASCE)0733-9445(1988)114:5(1019).

55. W. K. Tso, T. J. Zhu, and A. C. Heidebrecht, "Engineering Implication of Ground Motion A/V Ratio," *Soil Dynamics and Earthquake Engineering* 11, no. 3 (1992): 133–144, https://doi.org/10.1016/0267-7261(92)90027-B.

56. M. De Iuliis, E. Miceli, and P. Castaldo, "Machine Learning Modelling of Structural Response for Different Seismic Signal Characteristics: A Parametric Analysis," *Applied Soft Computing* 164 (2024): 112026, https://doi.org/10.1016/j.asoc.2024.112026.

57. M. De Iuliis, E. Miceli, and P. Castaldo, "Information Theory-Guided Machine Learning to Estimate Seismic response of Non-Linear SDOF Structures," *Engineering Structures* 336 (2025): 120448, https://doi.org/10.1016/j.engstruct.2025.120448.

scihm, 2026, 1, Downloaded from https://onlinelibrary.wiley.com/doi/10.1155/stc/8260623 by M. De Iuliis - Politecnico Di Torino Sist. Bibl Del Polit Di Torino , Wiley Online Library on [13/08/2026]. See the Terms and Conditions (https://onlinelibrary.wiley.com/terms-and-conditions) on Wiley Online Library for rules of use; OA articles are governed by the applicable Creative Commons License

58. CSI (Computers and Structures, Inc.), in *SAP2000—Integrated Software for Structural Analysis and Design* (Computers and Structures, 2023), https://www.csiamerica.com/products/sap2000.

59. MathWorks, "MATLAB (Version R2025a)," (2025), https://www.mathworks.com/products/matlab.html.

60. L. F. Shampine and M. W. Reichelt, "The MATLAB ODE Suite," *SIAM Journal on Scientific Computing* 18, no. 1 (1997): 1–22, https://doi.org/10.1137/S1064827594276424.

61. H. M. Hilber, T. J. R. Hughes, and R. L. Taylor, "Improved Numerical Dissipation for Time Integration Algorithms in Structural Dynamics," *Earthquake Engineering and Structural Dynamics* 5, no. 3 (1977): 283–292, https://doi.org/10.1002/eqe.4290050306.

62. S. Song and G. Li, "Inelastic Dynamic Analysis of Steel Structure Using Force Analogy Method," *Applied Mechanics and Materials* 166-169 (2012): 304–309, https://doi.org/10.4028/www.scientific.net/AMM.166-169.304.

63. S. Safaei, A. Taslimi, and P. Tehrani, "A Study on the Accuracy of Force Analogy Method in Nonlinear Static Analysis," *Structural Design of Tall and Special Buildings* 28, no. 13 (2019): e1654, https://doi.org/10.1002/tal.1654.

64. Taylor Devices, "Fluid Viscous Dampers: Specifications and Applications for Structural Control," (2024), https://www.taylordevices.com/products/fluid-viscous-dampers/.

65. JFE Steel Corporation, "Seismic Control Systems Using Buckling Restrained and Variable Stiffness Braces," (2021), https://www.jfe-steel.co.jp/.

66. D. Karnopp, M. J. Crosby, and R. A. Harwood, "Vibration Control Using Semi-Active Force Generators," *Journal of Engineering for Industry-Transactions of the ASME* 96, no. 2 (1974): 619–626, https://doi.org/10.1115/1.3438373.

67. D. Karnopp, "Design Principles for Vibration Control Systems Using Semi-Active Dampers," *Journal of Dynamic Systems, Measurement and Control, Trans. of ASME* 112, no. 1990 (1990): 448–454, https://doi.org/10.1115/1.2896163.

68. M. Ahamadian, "On the Isolation Properties of Semiactive Dampers," *Journal of Vibration and Control* 5, no. 1999 (1999): 217–232, https://doi.org/10.1177/107754639900500204.

scihm, 2026, 1, Downloaded from https://onlinelibrary.wiley.com/doi/10.1155/stc/8260623 by M. De Iuliis - Politecnico Di Torino Sist. Bibl Del Polit Di Torino , Wiley Online Library on [13/08/2026]. See the Terms and Conditions (https://onlinelibrary.wiley.com/terms-and-conditions) on Wiley Online Library for rules of use; OA articles are governed by the applicable Creative Commons License